Journal of Hazardous Materials Advances 23 (2026) 101389

Contents lists available at ScienceDirect

Journal of Hazardous Materials Advances

journal homepage: www.elsevier.com/locate/hazadv

Phenyl carbon nitride-based self-cleaning coatings: A sustainable solution for indoor air quality management

Stefania Porcu, Moulika Hazra *, Riccardo Lodo, Daniele Chiriu, Pier Carlo Ricci

Department of Physics, University of Cagliari, Monserrato, Complesso Universitario di Monserrato S.P. Monserrato-Sestu Km 0, 700 09042, Monserrato, CA, Italy

ARTICLE INFO

Keywords:
Carbon nitride
TiO_2
Photocatalysis
Indoor pollution
Cigarette smoke
Building materials
PAHs
Cultural heritage

ABSTRACT

Indoor-air pollution in public spaces and homes due to wood burning and cigarette smoking has increased the concentration of carcinogenic polycyclic aromatic hydrocarbons (PAHs) and carbonaceous soot in the air being continuously inhaled. These non-volatile compounds not only threaten the health of the humans and animals breathing that air but also deteriorates the cultural heritage artifacts and general infrastructure which would then need regular maintenance and painting. Anti-pollution paints and coatings containing TiO_2 have been recently applied to manage these challenges which utilize energy-intensive UV light sources for their photocatalytic activation. Therefore, there is a need for visible-light active technologies which could mitigate the problems related to indoor air management. We report an inorganic-organic heterostructure based on the industrially utilized TiO_2 and a phenyl-modified carbon nitride (PhCN), which demonstrates self-cleaning properties from wood smoke and cigarette smoke under a white LED lamp irradiation. This hybrid photocatalyst showed an efficient degradation of the organic pollutant dye Methyl Orange with a rate of 0.665×10^{-2} min^{-1} and Rhodamine B with a rate of 2.34×10^{-2} min^{-1} under visible light. The photocatalytic degradation of carbon-based matter in the smokes of wood and cigarette was monitored by reflectance measurements, colorimetric analysis and Raman Spectroscopy. The self-cleaning efficiencies of the TiO_2/PhCN coatings were found to be 76.8% for wood smoke and 68.5% for cigarette smoke in 6hours under a white LED lamp. This PhCN sensitized TiO_2 material holds promise as a UV-free indoor coating/paint for smoke abatement.

1. Introduction

Indoor air quality (IAQ) has become a critical public health and environmental concern in the modern era. Recent studies indicate that people spend approximately 80% of their time in enclosed environments such as homes, offices, schools, and public buildings. (Baeza_Romero et al., 2022) These confined spaces often contain elevated concentrations of volatile organic compounds (VOCs), polycyclic aromatic hydrocarbons (PAHs), carbon monoxide, nitrogen oxides, particulate matter (PM), and other harmful species derived from human activity, cleaning agents, and building materials. (Mehta et al., 2023; Yang et al., 2025; Mai et al., 2024) Indoor pollution can originate from various sources, including cigarette smoke, wood-burning fireplaces, gas stoves, carpets and upholstery fabrics, paints, cleaning products, perfumes, scented candles, building materials and furnishings, electronic devices, and building maintenance products. (Buonanno and Kumar, 2025; Kim et al., 2022; Sangkham et al., 2024) Cigarette smoke remains one of the most persistent and hazardous sources of indoor pollution, contributing to the emission of over 7000 chemicals, including volatile sulphur compounds, formaldehyde, benzene, and polycyclic aromatic hydrocarbons (PAHs). (Nagarajan and Chandiramouli, 2019) It is reported that approximately 20% of the world's population are smokers. Long-term exposure to these pollutants even in the form of second-hand and third-hand smoke has been directly linked to respiratory diseases, cardiovascular problems, and even carcinogenesis. (Soleimani et al., 2022) Thus, not smoking cigarettes does not safeguard someone from its negative effects. Burning of wood for cooking and heating purposes at homes or public spaces, results in aesthetic damages, reduced visibility, in addition to contributing to lung infections in humans. According to Centers for Disease Control and Prevention, people exposed to wood smoke have a higher difficulty rate in recovering from COVID-19. (Wood Smoke and Your Health, 2025) It contains benzene, formaldehyde, acrolein and polycyclic aromatic hydrocarbons (PAHs) and particulate matter (PM) which are toxic in nature. (Wood Smoke and Your Health,

* Corresponding author.
E-mail addresses: stefania.porcu@dsf.unica.it (S. Porcu), moulika.hazra@unica.it (M. Hazra), riccardolodo99@gmail.com (R. Lodo), daniele.chiriu@dsf.unica.it (D. Chiriu), carlo.ricci@dsf.unica.it (P.C. Ricci).

https://doi.org/10.1016/j.hazadv.2026.101389
Received 15 April 2026; Received in revised form 8 June 2026; Accepted 10 July 2026
Available online 10 July 2026

2025)

To prevent these negative effects due to PMs, VOCs, PAHs, etc., there have been recent reports of several techniques such as triboelectric nanogenerator, biofiltration, air ionizing, nonthermal plasma, photocatalytic oxidation and more, which aim to either physically remove the non-volatile pollutants or decompose the volatile ones into harmless products. (Nagarajan and Chandiramouli, 2019; Sheoran et al., 2022; Weon et al., 2019; Talaie et al., 2026; Singh et al., 2024) The search for advanced technologies to combat indoor air pollution also involves selecting environmentally friendly, low-energy, and easily implementable methods that utilize earth-abundant and inexpensive materials. (Singh et al., 2024) These criteria are essential for large-scale application of the IAQ management technology. Photocatalysis offers a promising route for the decomposition of airborne pollutants through light-induced redox reactions. (He et al., 2021) When irradiated by a light source with energy higher than the bandgap of the photocatalyst, electron-hole pairs are generated in the photocatalyst that react with oxygen and water molecules to produce reactive oxygen species (ROS), such as hydroxyl radicals and superoxide ions. These reactive species can oxidize pollutants into harmless end products like CO_2 and H_2O. (Hazra et al., 2025) Conventional photocatalytic materials have been extensively studied due to their high stability and proven ability to degrade a wide range of organic and inorganic contaminants whether in air or water. (Vasiljević et al., 2025; Myakala et al., 2024; Porcu et al., 2023) This multipurpose ability of photocatalysts has newly been ported to develop anti-pollution paints, coatings and building materials which tackle with the air pollutants and the wear and tear of infrastructure. (Mills et al., 2014; Stefanakis et al., 2021; Krishnan et al., 2018; Munafò et al., 2014; Khannyra et al., 2022; Dudek and Janus, 2022)

Among the photocatalytic materials demonstrating superior performance, n-type semiconductors such as TiO_2, WO_3, and Fe_2O_3 are the most widely used. (Yang et al., 2025; Mayouf et al., 2025; Samuel et al., 2022) Titanium dioxide is one of the photocatalysts that garners the most interest due to its high performance compared to others in terms of stability, low toxicity, low cost, ease of synthesis, and good photocatalytic activity. Furthermore, its strong oxidizing capacity has made it one of the most studied and utilized photocatalytic material. (Yang et al., 2025; Anucha et al., 2022; Armaković et al., 2022) However, the application of TiO_2-based photocatalysts in indoor environments faces significant limitations. The most notable drawback is that TiO_2 exhibits a wide bandgap (~3.2 eV), which restricts its activation to the UV region, accounting for only 3–5% of the solar spectrum and virtually absent in standard indoor lighting. (Hazra et al., 2025) Existing market products rely primarily on TiO_2-based formulations that demand UV activation, often supplied by artificial UV lamps that are energy intensive or sunlight exposure. (Munafò et al., 2014; Tang et al., 2024) For indoor environments where lighting is predominantly from visible or warm-white LED sources, such TiO_2 is largely ineffective. Additionally, the cost of high-quality photocatalytic paints remains prohibitive, preventing their widespread adoption in residential and commercial buildings. (Wu et al., 2022).

To address this issue, various methodologies have been tested for modifying TiO_2 to utilize visible light and make it more suitable for indoor photocatalysis– doping with metals, doping with non-metals, surface modification and hybrid formation. (Ishaq et al., 2024; Khan et al., 2025; Nimmy et al., 2025) Specifically, hybridization with materials like CdS, CdSe quantum dots, noble metals, graphene, g-C_3N_4, to form photocatalytic heterostructures has proven its efficiency in engineering the band gap of TiO_2 for visible light utilization. (Ishaq et al., 2024; Roongraung et al., 2023; Dettori et al., 2025) However, these common visible-light sensitizers present significant drawbacks, including toxicity and photocorrosion (CdS, CdSe), high cost and instability (noble metals), limited intrinsic photoactivity (graphene, rGO), and poor durability with leaching issues (organic dyes). (Wang et al., 2026; Yang et al., 2023; Misra et al., 2023; Alsharief et al., 2026) Therefore, we must be cautious while choosing a visible light sensitizer for TiO_2 so as not to be counterproductive while managing IAQ. Carbon nitrides do not pose the above challenges to photocatalysis on a material level. They are metal-free, chemically stable, non-toxic, earth-abundant and visible-light active, and are therefore suitable for sustainable applications. In addition, the graphitic structure and nanolayer arrangement of carbon nitrides makes them ideal for thin films and coatings applications. (Higazy et al., 2025) Recent advances in the modification of carbon nitride with aromatic or phenyl groups have further enhanced its optical absorption and charge separation efficiency. (Bagchi et al., 2026; Hazra et al., 2025) The incorporation of phenyl groups into the carbon nitride framework modifies its electronic structure and extends the π-conjugated network, thereby enhancing light absorption, particularly in the visible region. (Porcu et al., 2020) The electron-rich aromatic rings of the phenyl groups facilitate charge transfer and suppress the recombination of photogenerated electron-hole pairs. (Porcu et al., 2020; Ghourichay and Ricci, 2026) Consequently, this modification improves the photocatalytic performance of carbon nitride in applications such as hydrogen evolution and pollutant degradation, while also enhancing its structural stability under reaction conditions. (Hazra et al., 2025; Hazra et al., 2025) However, it still exhibits a high photoluminescence under visible-light and a low surface area and porosity, which hampers the photocatalytic ability of phenyl-modified carbon nitride (PhCN). (Bagchi et al., 2026) Nonetheless, PhCN can serve as the visible light sensitiser for TiO_2 to form a hybrid photocatalyst that combine the best features of both materials: the stability and charge transport of TiO_2 with the visible-light activity of the organic phase. (Porcu et al., 2022)

The central problem addressed in this article is the development of a cost-effective, visible-light-active, and durable photocatalytic coating capable of degrading indoor air pollutants, specifically cigarette smoke and wood smoke components, under common indoor lighting conditions. This goal was achieved through the creation of a hybrid inorganic-organic photocatalytic system that exploits synergistic interactions between TiO_2 nanoparticles and phenyl-modified carbon nitride (PhCN) polymer. The heterostructure was synthesized through a facile solvothermal method which could be easily replicated on a big scale. PhCN successfully acted as a visible-light sensitizer for the TiO_2. The heterostructure was efficient in degrading the common organic dye pollutant RhodamineB (RhB) with a degradation rate of 2.34×10^{-2} min^{-1} under a white light LED lamp, which showed its efficiency in interacting with organic molecules. Tests were conducted for the removal of pollutants from wood and cigarette smoke by the TiO_2/PhCN coatings under visible-light irradiation and the efficiency was found to be 76.8% and 68.5% respectively in 6 h. Diffused reflectance spectroscopy (DRS), Colorimetry and Raman spectroscopy were all implied to confirm the particulate matter detection and carbonaceous matter removal by the photocatalytic coatings which showed self-cleaning properties and colour maintenance.

A successful demonstration of cigarette and wood smoke degradation under ordinary LED illumination marks a substantial advancement in indoor air purification technologies. This demonstrates the advantage of utilising hybrid heterostructures in providing a cost-effective and sustainable alternative to UV-dependent photocatalytic paints. The development of such photocatalytic coatings has far-reaching implications across multiple domains: residential and commercial buildings as wall paints, wallpapers, or tiles to continuously purify indoor air, particularly in urban environments with limited ventilation; in healthcare facilities to maintain a healthy environment for patients staff; cultural heritage preservation from pollutant-induced deterioration of artworks and documents; and other public spaces like- airports and industrial offices where air quality is a persistent concern, providing passive purification without external power input. The integration of visible-light active photocatalytic coatings with existing lighting systems also aligns with the global agenda of sustainable development, reducing the need for energy-intensive air purification equipment.

This work with TiO_2/PhCN system stands at the intersection of materials science, surface engineering, and environmental technology. This approach builds on the proven stability of TiO_2 while incorporating the tunable optoelectronic properties of organic semiconductor PhCN, representing a new paradigm in photocatalytic paint design.

2. Experimental section

2.1. Materials

2,4-diamino-6-phenyl-1,3,5-triazine ($C_6H_5(C_3N_3)(NH_2)_2$, Ph-Triazine,99%, Sigma Aldrich), Titanium tetrachloride ($TiCl_4$,99%, Sigma-Aldrich), Absolute ethanol(C_2H_5OH,96%,Alfa Aesar), RhodamineB (RhB,$C_{28}H_{31}ClN_2O_3$, 95%,Sigma-Aldrich), Methylene Blue(MB, $C_{16}H_{18}ClN_3S$,Millipore Corp), Methyl Orange (MO,$C_{14}H_{14}N_3NaO_3S$, Sigma-Aldrich). All chemicals were used as received without further purification. All chemicals were used as received without further purification. Deionized (DI) water was used in the preparation of the Rhodamine aqueous solution. (Porcu et al., 2020)

2.2. Synthesis of PhCN

The phenyl-modified Carbon nitride (PhCN) was prepared by heating 1 g of 2,4-diamino-6-phenyl-1,3,5-triazine powder (Ph-Triazine) in a closed glass container in a muffle furnace at 400 °C for 2 h in the presence of air. The heating rate was kept at 10 °C/min and the cooling at 5 °C/min.

2.3. Synthesis of TiO_2

Anatase TiO_2 sample was prepared via solvothermal method in 20 ml ethanol and 0.5 ml of $TiCl_4$ for reference measurements.

2.4. Preparation of TiO_2/PhCN

The PhCN (100 mg) was stirred at room temperature for 30 min in 20 ml of ethanol. Subsequently, 0.5 ml of $TiCl_4$ was added and the solution was stirred at room temperature for 2 h. The resulting solution was then transferred into a Teflon autoclave and heated at 180 °C for 8 h. Following the reaction, the product was filtered and subjected to multiple washes with deionized water and absolute ethanol. The washed sample was then dried at 60 °C for 12 h. (Porcu et al., 2020)

2.5. Preparation of TiO_2/PhCN coatings

Different amounts of hybrid photocatalyst powders from 2 mg to 30 mg were dissolved in 100 μL of ethanol in a test tube to obtain different concentrations of the dispersion after 10 min of sonication. Then they were drop-casted on a glass slide inside the surface area of 1.5 cm^2. The sample with the most uniform coating was chosen for further experiments, i.e. 20 mg of TiO_2/PhCN in 100 μL of ethanol. The sample was then left to dry before use, allowing the ethanol to evaporate, leaving only the hybrid material on the slide.

The whole process of the preparation of the photocatalytic coating is shown in the Fig. 1.

2.6. Smoking of the coatings

All smoke exposure processes, designed to replicate the effects of exposure to cigarette and wood smoke, were conducted using a handmade smoking apparatus, consisting essentially of two components: the smoking chamber and the smoker joined by a connector. The chamber is sealed completely and kept away from light, ensuring that they effectively undergo the effects of smoke exposure. Smoke is generated by the combustion of tobacco or wood placed in a designated opening in the smoker, a device connected to the chamber that draws in the smoke and transports it to the area where the samples are located. This process is schematically presented in Fig. 2.

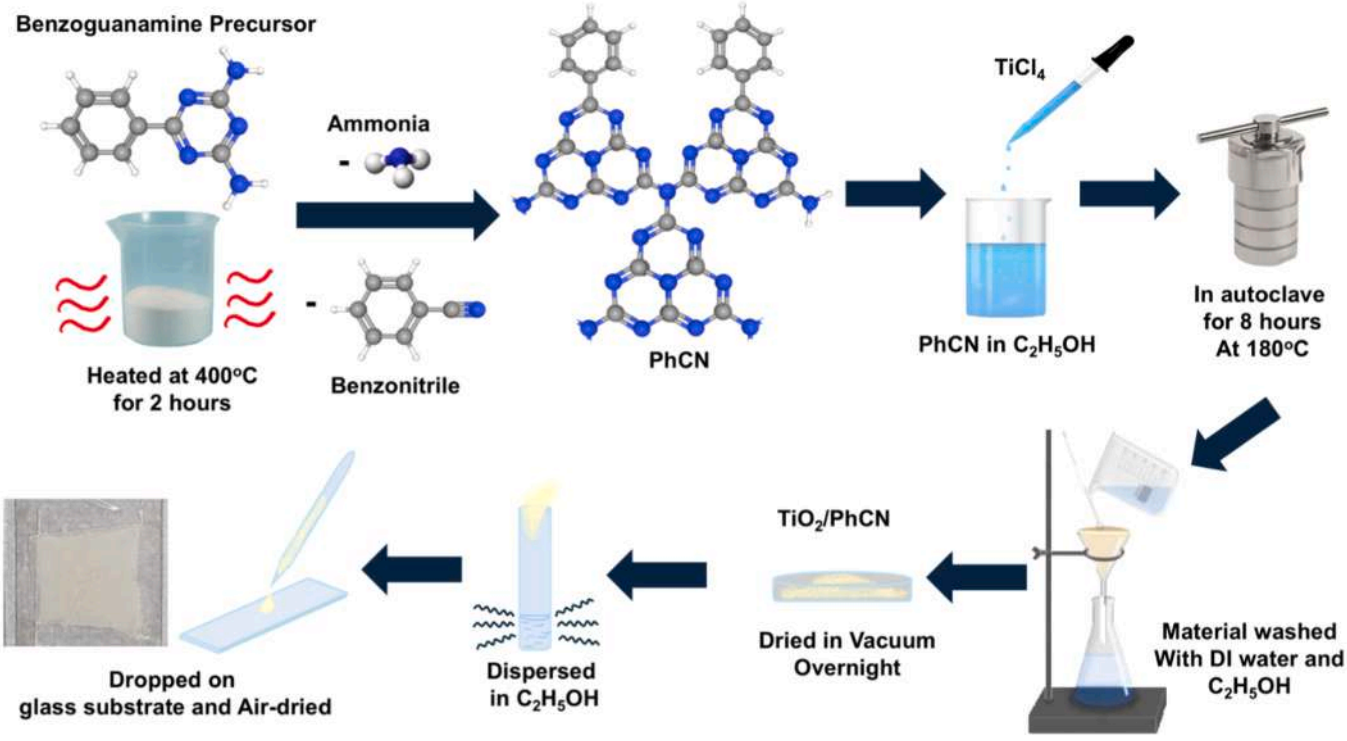

Fig. 1. Schematic for the preparation of the photocatalytic coating.

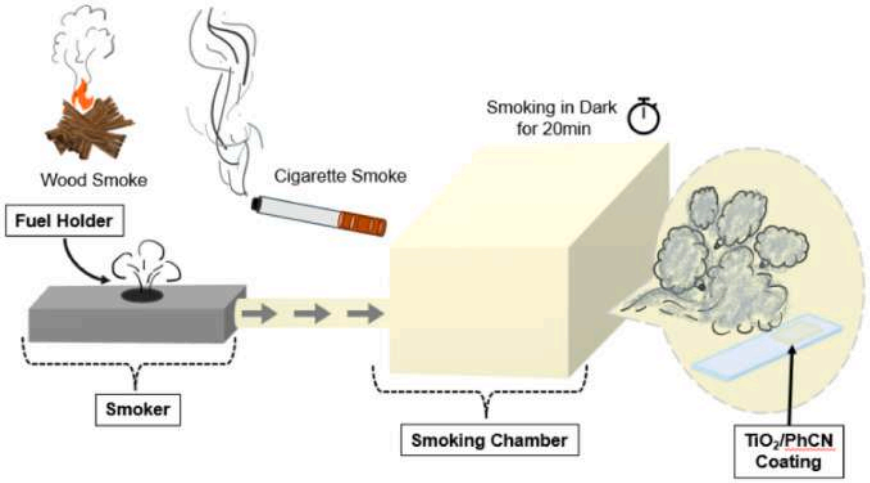

Fig. 2. Schematic representation of the smoking of the photocatalytic coatings.

2.7. Characterization techniques

2.7.1. X-Ray diffraction

X-ray diffraction patterns were collected at room temperature by using a Rigaku Miniflex II diffractometer with θ−2θ Bragg-Brentano geometry with Cu Kα (λ = 1.5418 Å), radiation at room temperature.

2.7.2. Fourier-transform infrared spectroscopy

Spectrum Two FT-IR Spectrometer from Perkin Elmer was used to acquire the infrared spectra of all the hybrids and pristine samples ($LiTaO_3$ detector, scan range 4000–450cm^{-1}).

2.7.3. Raman measurements

For TiO_2 samples, the Raman measurements were done in the backscattering geometry using the 532 nm line sourced from a wavelength stabilized diode module (LASOS DPSS series) that is coupled to a Reflecting Bragg Grating (Optigrate-Braggrade 532) to narrow the laser linewidth. Measurements were performed at room temperature with a Raman spectrometer MS-750 Sol Instruments system with a spectral resolution of 1 cm^{-1}. Spectra were recorded in the Stokes region using a 1200 groove·mm^{-1} grating monochromator.

In-situ micro Raman scattering measurements were carried out in back scattering geometry with the 1064 nm line of an Nd:YAG laser for PhCN and the hybrid. Measurements were performed in air at room temperature with a compact spectrometer B&WTEK (Newark-USA) i-Raman Ex integrated system with a spectral resolution of 8 cm^{-1}. For the photocatalytic tests, with each experimental setup, all the spectra were collected with an acquisition time of about 60 s (five replicas) and power excitation between 5 and 10 mW concentrated in a spot of 0.3 mm^2 on the surface through a Raman Video Micro- Sampling System (Nikon Eclipse for high-resolution and BAC151B in the other case) equipped with a 20 × Olympus objective to select the area on the samples. These conditions were selected after preliminary studies as safe conditions for the samples. Each Raman test was repeated three times to verify result reproducibility.

2.7.4. Scanning electron microscopy

SEM studies were carried out using a Carl ZEISS Auriga microscope equipped with an energy dispersive X-ray spectroscopy (EDX) detector or an ESEM FEI Quanta 200 microscope operating at 30 KV.

2.7.5. Transmission electron microscopy

Transmission Electron Microscope TEM JeolJEM 1400 Plus was used for bright field imaging of TiO_2 nanoparticles, PhCN nanosheets and the TiO_2/PhCN as-prepared hybrids under ultra-high vacuum conditions.

2.7.6. Diffused reflectance measurements

UV–Vis-NIR solid-state absorbance/reflectance spectra were collected (applying baseline corrections) by a Jasco V-750 spectrophotometer with a spectral bandwidth of 2 nm in the 200–800 nm range.

2.7.7. Steady state photoluminescence

PL measurements were performed with an excitation wavelength of 405 nm coupled to an Avantes Sensilne Avaspec-ULS-TEC Spectrometer with an optical fiber. The measurements were recorded for a spectral range of 300–900 nm with a 100 ms time window.

2.7.8. Time resolved photoluminescence (TRPL)

Time-resolved photoluminescence (TR-PL) measurements were performed by exciting the samples with 410 nm by an optical parametric amplifier (Light Conversion TOPAS-C) pumped by a regenerative Ti: Sapphire amplifier (Coherent Libra-HE, Coherent Inc., Santa Clara, CA, USA). The repetition frequency was 1 kHz, and the PL signal was recovered by a streak camera (Hamamatsu C10910, Hamamatsu Photonics, Hamamatsu City, Shizuoka Pref., Japan) equipped with a grating spectrometer (Princeton Instruments Acton SpectraPro SP-2300, Teledyne Princeton Instruments, Trenton, NJ, USA).

2.7.9. Colorimetric analysis

The CIE L*,a*, b* coordinates and the total color variation ΔE were extracted from reflectance spectra Collected by means of an integrating sphere and with a geometry of 10° The results were related to the D65 illuminant and the CIELab standard colorimetric observables. The CIE coordinates were obtained using the ColorConvert v. 7.77 software.

The coordinates in this color space are as follows:

- L* represents brightness, indicating the position on the vertical axis from black (L* = 0) to white (L* = 100) and is always positive.
- The values of a* and b* define the chromaticity of the color and can take both positive and negative values. The respective axes of a* and b*, perpendicular to each other, intersect on the L* axis.

The total color variation (△E) has been calculated following the formula:

$$\Delta E^* = \sqrt{(\delta L^*)^2 + (\delta a^*)^2 + (\delta b^*)^2}$$

2.8. Measurement of the photocatalytic dye-degradation activity

The photocatalytic performance of the hybrid TiO_2/PhCN was first evaluated by monitoring the concentration changes in a Rhodamine B

aqueous solution under visible light irradiation. The photocatalytic performance was assessed using a white LED (white LED 11 W, 6 mW/cm^2) as the light source. Before light irradiation, both the catalyst suspension (50 mg) and RhB (50 mL, 10 mg·L^{-1}) were stirred in the dark for 30 min to ensure absorption-desorption equilibrium between the catalyst and the dye. During the photodegradation process, 2 ml aliquots were collected every 60 min. The aliquots were then centrifuged and the residual concentrations of RhB were analyzed using the Beer-Lambert Law to determine the degradation rate of the process-

$$A = \varepsilon c l$$

Where, A is the absorbance of the solution, ε is the absorption coefficient of RhodamineB, c is the concentration of RhB in the sample and l is the thickness of the cuvette.

More dye degradation tests were conducted with Methyl Orange (MO) and Methylene Blue (MB) dyes with the same concentrations of 10 mg L^{-1} and same process to better understand the surface phenomena. The rate of degradation of the dyes by the photocatalyst was calculated by the pseudo-first order kinetics:

$$-ln\left(\frac{c_0}{c_t}\right) = kt$$

Where c_0 is the initial dye concentration, c_t is the concentration of the dye at time t and k is the rate constant of the dye degradation.

2.9. Photocatalytic degradation of smoke

The glass substrate with the photocatalytic TiO_2/PhCN coating was put inside the handmade smoking chamber and then was subjected to cigarette and wood smoke separately for a continuous 30 min. After smoking, the samples were taken out from the chamber and then put under LED light bulb with a white light emission for different amounts of times (2 h, 4 h, 6 h and 18 h). The samples were named as: coating without any smoke exposure T_x, coating after the smoke exposure T_0, coating after 2 h light exposure T_2, coating after 4 h light exposure T_4 and so on. The samples under the wood smoke were prefixed with W_ and the ones under cigarette smoke with C_.

The degradation process was studied through measurements of reflectance, colorimetric analysis, and Raman spectroscopy of the samples– W_T_x, W_T_0, W_T_2, W_T_4, W_T_6, W_T_{18} and C_T_x, C_T_0, C_T_2, C_T_4, C_T_6, C_T_{18}

The samples were subjected to multiple photocatalytic cycles to assess stability and/or durability.

3. Results and discussion

3.1. XRD

After the preparation of TiO_2 and PhCN powders, firstly structural characterizations were performed to verify their chemical phases. XRD was performed on TiO_2, PhCN and TiO_2/PhCN powder samples to study their crystalline content and look for any probable secondary phases. Fig. 3a shows the X-ray diffractograms of all three samples. The

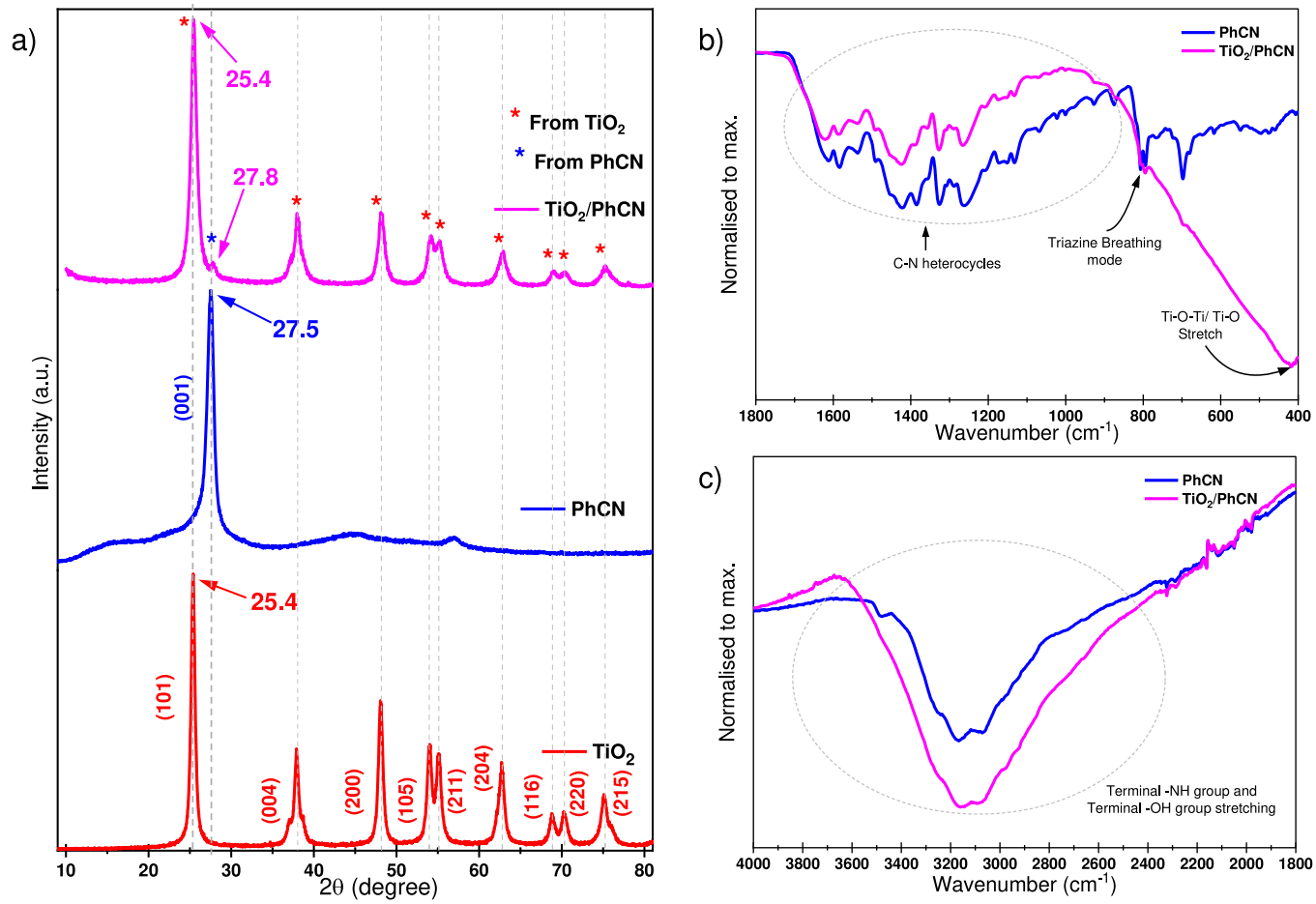

Fig. 3. a) X-ray diffractograms of the pristine PhCN, TiO_2 and the TiO_2/PhCN hybrid. b) ATR-FTIR transmittance of the samples from 1800–400 cm^{-1},c) from 4000–1800 cm^{-1}.

crystallographic planes of (101), (004), (200), (105), (211), (204), (116), (220) and (215) for the prepared TiO_2 powder confirmed the preparation of the tetragonal anatase phase of the Titania (TiO_2), without any peaks from rutile or brookite phases. (Hazra et al., 2025) This anatase phase is majorly credited for its high photocatalytic activity and stability which was intended for this study. (Hazra et al., 2025; Dettori et al., 2025) The PhCN showed a semi-crystalline behaviour with a well-defined peak at 27.5°, corresponding to the (001) reflection in carbon nitrides related to the interlayer spacings of nanosheets. (Hejazi et al., 2024) Additionally, a broader peak is observed from 13°−20°, attributed to the reflection originating from the (210) plane which is related to the in-plane repeating motifs. (Hazra et al., 2025; Durmus et al., 2025) The hybrid TiO_2/PhCN shows all the characteristic peaks of both the components emphasizing the achievement of the hybrid system. The (001) peak of PhCN is moved to 27.8 in the hybrid system, this increase in the reflection angle suggests a decrease in the D-spacing of the PhCN nanosheets due to the incorporation of TiO_2. The deposition of TiO_2 nanocrystals on the surface of PhCN during the high-pressure solvothermal synthesis leads to a close stacking of the PhCN nanosheets. The intensity of the peak related to PhCN is observed to be much lower than those corresponding to TiO_2, due to the high crystalline nature of the anatase, along with the higher amount of TiO_2 in the hybrid. From our measurements, the mass ratio of PhCN:TiO_2 in the hybrid is 2:6.

The crystallite sizes of the TiO_2 and TiO_2/PhCN were calculated after fitting the most prominent peak in XRD with a pseudo-voigt function (Figure S1) to obtain the full width at half maximum (β) of the diffraction peak (in radians) at the Bragg angle θ. The Scherrer equation was used for this calculation:

$$D = \frac{k\lambda}{\beta\cos\theta}$$

Where, D is the average crystallite size; K is the shape factor, typically around 0.9; λ is the incident X-ray wavelength in nm. The average crystallite size of the crystalline TiO_2 was found to be 15.2 nm and that of the hybrid was 10.14 nm. These values suggest that TiO_2 forms smaller crystallites when PhCN is present in the autoclave. This can also lead to less available volume available for the TiO_2 and subsequent higher pressure leading to an overall smaller TiO_2 crystallite distribution in the hybrid.

3.2. ATR-FTIR

To investigate the organic part of the hybrid (PhCN) well, FTIR spectroscopy was conducted on the samples, and the results are shown in Fig. 3b and c. PhCN exhibits distinct vibrational features associated with its carbon-nitrogen framework. The bands observed at 1383, 1324, and 1250 cm^{-1} are attributed to sp^3 C–N stretching modes, while those at 1611 and 1534 cm^{-1} arise from sp^2 C═N vibrations, consistent with previously reported spectra. (Hazra et al., 2025) The peak at 810 cm^{-1} corresponds to the characteristic breathing mode of triazine rings, confirming their presence in the material. (Hazra et al., 2025) Additionally, the broad absorption spanning 3500–2400 cm^{-1} is assigned to physically adsorbed water leading to –OH on the surface and the smaller peaks at 3500–3000cm^{-1} are related to terminal N–H functionalities. (Hazra et al., 2025) All of these PhCN signatures are preserved in the hybrid TiO_2/PhCN without any shift however, the transmittance related to the CN heterocycles showed higher values. This demonstrates the deposition of TiO_2 on the surface of PhCN in the hybrid which prevents IR absorption by the organic part, leading a higher transmittance. The formation of TiO_2 in the hybrid is evidenced by the emergence of a broad low-wavenumber band around 483 cm^{-1}, characteristic of Ti–O lattice vibrations. (Hazra et al., 2025) The wider feature between 3500 and 2800 cm^{-1}, associated with surface – OH groups, becomes sharper and wider showing higher adsorption of water on the surface of the hybrid which could be beneficial for enhanced pollutant adsorption on the surface of this material.

3.3. Raman spectroscopy

Further structural study was carried out by performing Raman spectroscopy measurements for the samples. Fig. 4a depicts the normalized Raman response from pristine TiO_2 and the hybrid samples. TiO_2 has been reported to show the Raman E_g mode at 144 cm^{-1} and it is observable in both of the samples at 146 cm^{-1}. (Bersani et al., 1998) The Raman spectrum of PhCN is depicted by Fig. 4b where the organic signatures are observable as, $–NH_2$ mode at ~1000 cm^{-1}, the C–C stretch between the phenyl ring and the triazine ring, and the phenyl motion at 1601 cm^{-1}. (Porcu et al., 2020) The Raman signatures corresponding to the PhCN were masked in the hybrid by TiO_2. In Fig. 4a, a broadening of the E_g peak of TiO_2 is observed for the hybrid due to the incorporation of PhCN with TiO_2. According to the phonon confinement model (quantum confinement), this broadening depicts a smaller size of TiO_2 nanocrystals in the hybrid than the pristine TiO_2. (Bersani et al., 1998; Cappelletti et al., 2005) This conclusion is in accordance with the XRD results.

3.4. SEM

SEM images in Fig. 5a–c, offer a thorough understanding of the morphological features of the TiO_2/PhCN hybrid system. TiO_2 particles in Figure a, appear as spheres with different diameters. On the other hand, PhCN,in Fig. 4b, does not show any spherical features but a lamellar network with high agglomeration. PhCN does not exhibit well-defined particle boundaries unlike the crystalline TiO_2. The non-uniform contrast of the electron micrograph is typical of polymeric materials and is consistent with the 2D conjugated framework of carbon nitrides where weak van der Waals interactions drive re-aggregation after synthesis. (Döblinger et al., 2008) The hybrid TiO_2/PhCN shows the aggregation of spherical particles (probably TiO_2) but no PhCN like irregularity which is indicative of TiO_2 adherence on the surface of PhCN chunks. The average particle size of TiO_2 was measured to be around 1.95 μm, while that of the hybrid was around 1.08 μm. This indicates a higher aggregation for the TiO_2 which is minimised by the hybridization with PhCN. The smaller particle size also contributes towards a higher available surface area for effective photocatalysis.

3.5. EDS

The Energy dispersive spectroscopy provides an elemental analysis of the samples. TiO_2 shows the presence of high amounts of Ti signal and lower O with some Cl% which comes from the precursor $TiCl_4$ which might stay as a remnant (Figure S2a). The high carbon detection for TiO_2 comes from the underlying carbon tape which was caught up during the 150 μm^2 area raster scan. The PhCN sample shows only C and N in major amounts and a few O from surface adsorbed groups (–OH) as seen in the FTIR spectrum. There are no impurities detected in the carbon nitride (Figure S2b). The hybrid TiO_2/PhCN shows all the elemental species from the two components (Figure S2c). The EDS results in terms of atomic% of different elements are summarized in Table S1. Although the light atoms like C and N cannot be precisely measured in EDS, it can be observed that the hybrid shows a higher % of CN species than TiO species, suggesting that the TiO_2 inorganic part is higher in amount. This is also shown by XRD where the peaks related to TiO_2 were dominating in intensity. The stochiometric ratio of Ti:O in the hybrid is comparable to TiO_2 and this might also indicate the surface deposition of TiO_2 crystals on PhCN nanosheets.

3.6. TEM

To verify the structure of the hybrid, TEM microscopy was conducted

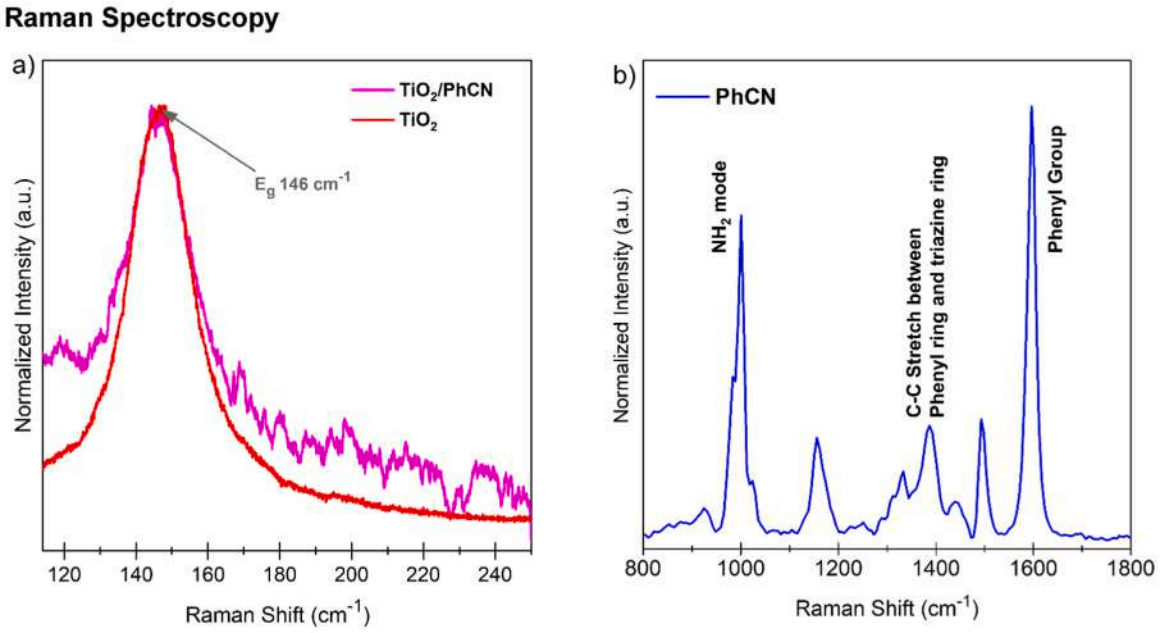

Fig. 4. Raman Spectra of a) TiO_2 and TiO_2/PhCN, b) PhCN.

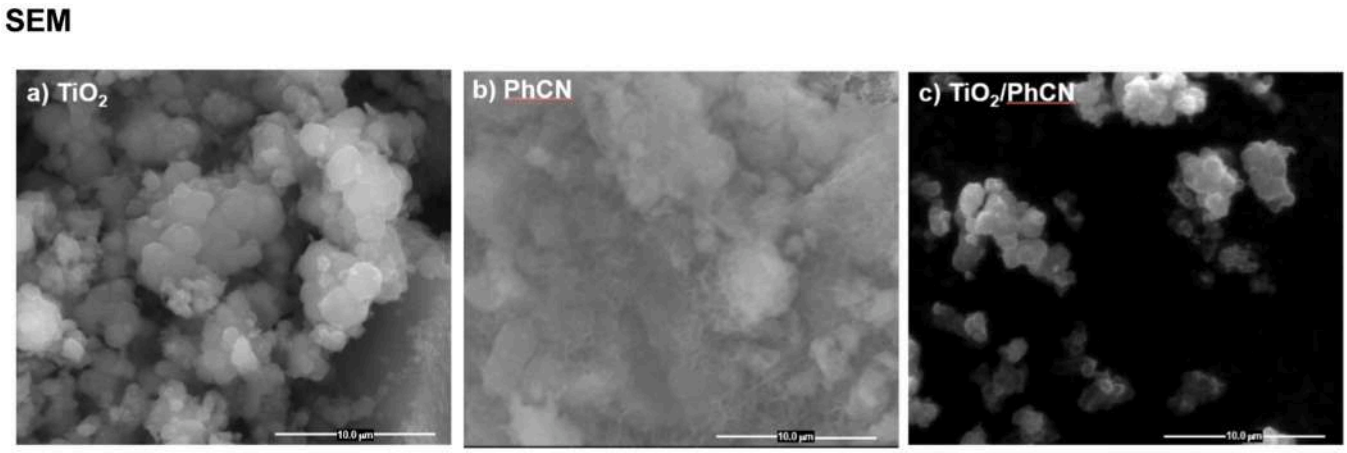

Fig. 5. SEM images of the samples a) TiO_2, b) PhCN, c) TiO_2/PhCN.

on the three samples as shown in Fig. 6a–c. The TiO_2 was clearly observed as a cluster of nanocrystallites in Fig. 6a whereas, PhCN did not show any crystallization and appeared as nanosheets stacked over one another (Fig. 6b). The TEM image of the hybrid in Fig. 6c showed the coverage of these PhCN nanosheets by the TiO_2 nanocrystals which could be seen as forming an envelope over the PhCN. This verifies our intentional design of core-shell structure of TiO_2/PhCN when we grew TiO_2 crystals on pre-synthesized PhCN via solvothermal synthesis. Here

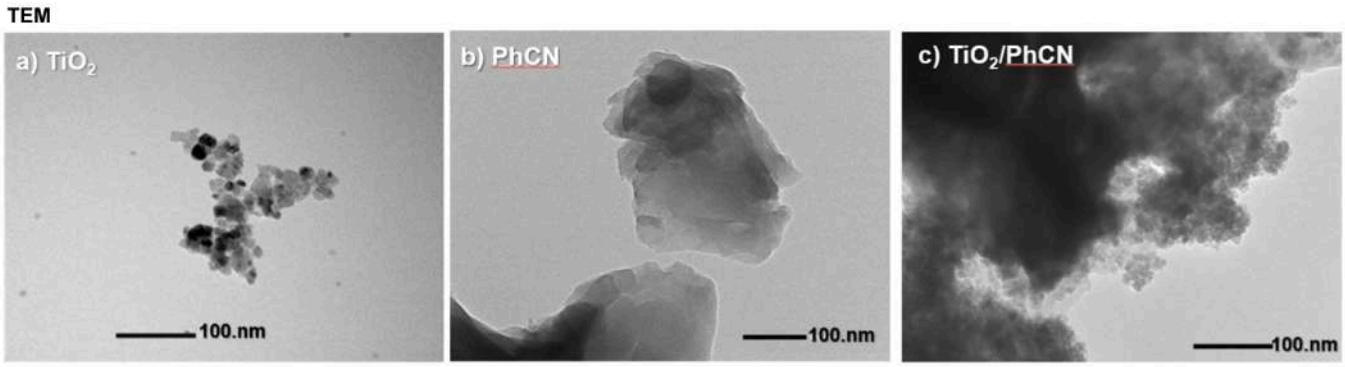

Fig. 6. TEM images of the samples a) TiO_2, b) PhCN, c) TiO_2/PhCN.

TiO_2 anatase acts as the shell (irregular) and PhCN as the core. The calculation of the average size of the nanodomains related to TiO_2 in the hybrid yielded 9.2 nm value, while the pristine TiO_2 sample showed nanodomains of average size of 12.35 nm. These values are in correspondence with the XRD-derived average crystallite sizes, where the pristine anatase showed a bigger structure than the anatase phase in the hybrid. Therefore, the TEM results show that the outer shell of the hybrid contains TiO_2 nanocrystals of smaller size, which may enhance the photocatalysis process by providing a higher surface area.

3.7. DRS

After understanding the structure and morphology of the hybrid, it is important to investigate the response towards the incident light for a photocatalytic material to ensure its spectral working range. DRS was employed with the excitation range of 300–600 nm, and the absorbance of the samples were normalized to the maxima and plotted in Fig. 7a using the Kubelka-Munk theory. The TiO_2 sample shows no absorption of light for wavelengths longer than 400 nm (visible range) and an absorption edge at around 390 nm with a high UV absorption. (Porcu et al., 2023) On the other hand, PhCN depicts a broad absorption range expanding in the visible spectrum with the maxima at around 420 nm. (Hazra et al., 2025) This enhanced visible-light absorption is provided by the presence of phenyl groups in the framework of carbon nitride. (Porcu et al., 2020) The phenyl group induces a redshift in the absorption edge of the carbon nitride, initiating light absorption at 600 nm and extending into the visible spectrum. Both components show their characteristic features in the hybrid where we can observe the absorption edge of TiO_2 at 390 nm and a visible-light absorption from the PhCN component. Hence, the resulting absorption spectrum represents a synergy of their individual contributions. Therefore, the hybrid system was interpreted as a weakly coupled heterojunction facilitating interfacial charge transfer. (Hazra et al., 2025)

The Fig. 7b–d show the Tauc plots of the materials where it is observed that the anatase shows its classic indirect optical bandgap of 3.2 eV, while PhCN shows a direct optical bandgap of 2.7 eV which is characteristic of carbon nitrides and matches the previously reported values. (Porcu et al., 2020; Stagi et al., 2016; Kokkotos et al., 2025) The Tauc plot analysis of the hybrid is done by considering it to be a modified TiO_2, as it is substantially higher in amount than PhCN. In addition, the DRS measurements and the structural characterizations do not show the formation of a new material or phase which could show novel energy bands. Therefore, the optical bandgap of such hybrid material does not symbolize brand-new energy bands but an alignment of the energy bands of the component materials. To obtain the apparent optical bandgap of the majority phase in the hybrid (anatase), a baseline correction was done using the linear contribution of the PhCN as the baseline (Fig. 7d). The TiO_2 in the hybrid exhibits an increase of 0.1 eV which can be assigned to the phenomenon of quantum confinement confirmed by the Raman measurements. (Xue et al., 2012) Nonetheless, this value of the optical bandgap is strictly restricted to the TiO_2 component of the hybrid as the plotting method treated the hybrid as a

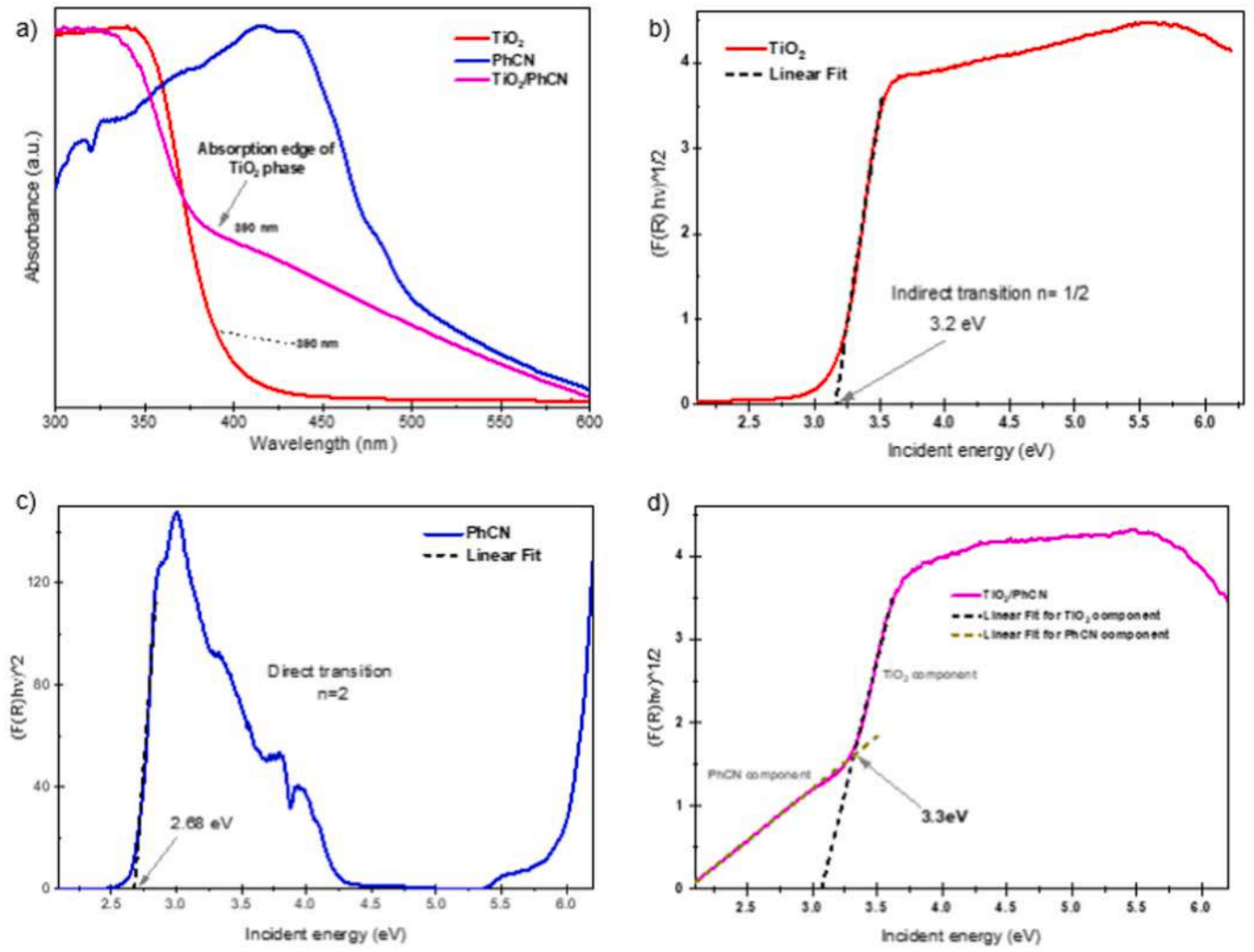

Fig. 7. a) Normalized absorption spectra of TiO_2, PhCN and TiO_2/PhCN. b), c) and d) Tauc plots of TiO_2, PhCN and TiO_2/PhCN respectively.

modified TiO_2 sample. This indicates the possibility of either a shift of the conduction band of TiO_2 to a higher level or a shift of the valence band to a lower level, or both. (Xue et al., 2012) However, Fig. 7d clearly shows the bandgap characters of both components present in the hybrid. Therefore, the presence of PhCN in hybrid would generate charge carriers with an incident light in the visible range of the light spectrum.

3.8. PL

The photocatalytic activity of a material is governed by the presence of photogenerated electrons and holes. From the previous section, it was confirmed that the hybrid had visible light absorption capabilities and hence can generate charge carriers under same excitation. These charge carriers should have a longer lifetime and less recombination rate to facilitate the surface redox reactions for photocatalysis. This can be studied by the photoluminescence measurements which provide the idea of radiative recombination of charge carriers in a sample. (Hazra et al., 2026) Therefore, the steady-state PL spectra of all the samples were measured under the 405 nm laser as we wish to utilize visible light for the photocatalytic reactions, and it is crucial to judge the materials under the same spectrum. Fig. 8a depicts a high intensity photoluminescence of PhCN centered at 530 nm and expanding from 400–800 nm. This broad emission from PhCN makes it an ideal candidate for white LED applications as reported previously. (Wang et al., 2022) However, this high radiative recombination is counterproductive for photocatalysis as it requires long-lived charge carriers which could be indicated by a lower intensity PL response. TiO_2 also shows a broad PL emission peaking at 610 nm which is attributed to surface and subsurface oxygen vacancies in the anatase phase (Fig. 8b). (Brüninghoff et al., 2019) However, the PL counts for TiO_2 is very low because of the low energy provided by the 405 nm laser which does not excite the UV active TiO_2 energy bandgap.

As observable in Fig. 8b, the PL spectrum of the hybrid shows the profile like that of PhCN with the maxima at 530 nm. There is no observable shift in the hybrid spectrum, while the profile shows broadening. The absence of a shift indicates little to no contribution in the PL from the TiO_2 component under 405 nm excitation, even if it is in a higher quantity. However, the profile broadening indicates a higher contribution from the highest and the lowest energy transitions in the PhCN component of the hybrid. Fig. 9a shows the energy transitions contributing to the total PL of PhCN which are $\sigma^* \rightarrow$ LP, $\sigma^* \rightarrow \pi$, $\pi^* \rightarrow$ LP , and $\pi^* \rightarrow \pi$. These four components can be observed in the deconvolution of the PL spectrum of the samples in Figure S3 a,b. A change in the % contribution from different bands were observed for the sample after hybridization with TiO_2. This can be due to a charge transfer to the conduction band of the TiO_2 from the LUMO of PhCN. This is further indicated by Fig. 8a, where the intensity of the PL spectrum of the hybrid was observed to be 10% of that of PhCN. This PL quenching of PhCN is due to the transfer of the photogenerated electrons under the visible-light excitation of 405 nm to the TiO_2 component, which makes it unavailable to transit it to the π and LP orbitals of PhCN. As there are now less electrons to relax to the ground states of π and LP, the intensity of PL declines. (Porcu et al., 2020) A low recombination of charge carriers in the hybrid shows a high expectation for photocatalytic activity.

3.9. TRPL

The charge transfer from PhCN to TiO_2 can be studied well with a time-resolved photoluminescence study which describes the mechanics of the charge-carrier recombination. Fig. 9b shows the TRPL spectra of PhCN and the hybrid taken under an excitation of 410 nm (visible light) with a time window of 1 μs. TiO_2 does not exhibit strong photoluminescence under this excitation to be caught by the detector. From the PL studies it was observed that the luminescence in the hybrid was due to the PhCN component, so the TRPL study of TiO_2 was not necessary. In Fig. 9b, it can be observed clearly that the hybrid TiO_2/PhCN presents an overall faster PL decay than PhCN. The decay profiles were further fitted with a multi-exponential decay function with 2 iterations–

$$y = y_0 + \sum_{i}^{2} A_i e^{-\frac{t}{\tau_i}}$$

The fitting provided us with the time constants related to the decay of the charge-carrier recombination in PhCN and the hybrid. The faster contribution is from the higher energy σ* level of PhCN with 8.97 ns time constant and the slower contribution is from the lower energy π* level with 87.54 ns time constant in PhCN. The higher energy contribution was faster in the hybrid to be 8.04 ns while the lower energy contribution is found to be 88.62 ns. However, the overall decay lifetime is longer for the hybrid.

The overall decay time obtained by the exponential decay fitting (τ_i) is related to the radiative lifetime contribution (τ_R), non-radiative lifetime contribution (τ_{NR}), probability for radiative recombination (γ_R) and the probability for non-radiative recombination (γ_{NR}) by the following

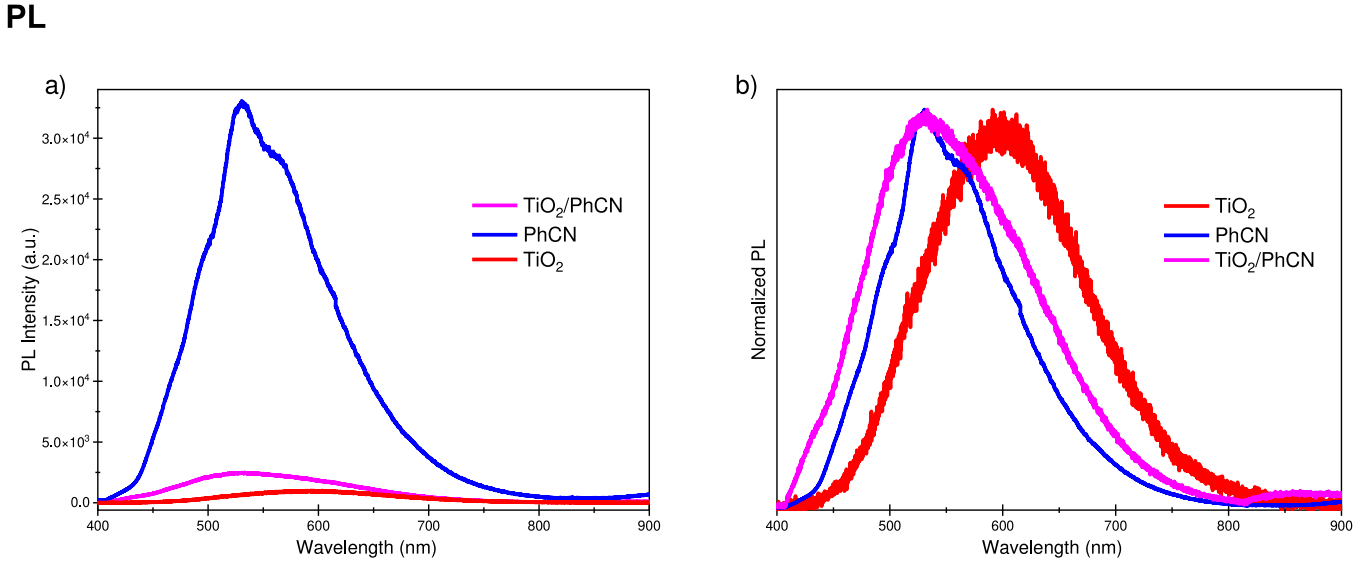

Fig. 8. Steady-state PL spectra of the samples under 405 nm LASER 100 ms response time a)With PL intensity as-measured, b) Normalized PL intensity of the samples to their maxima.

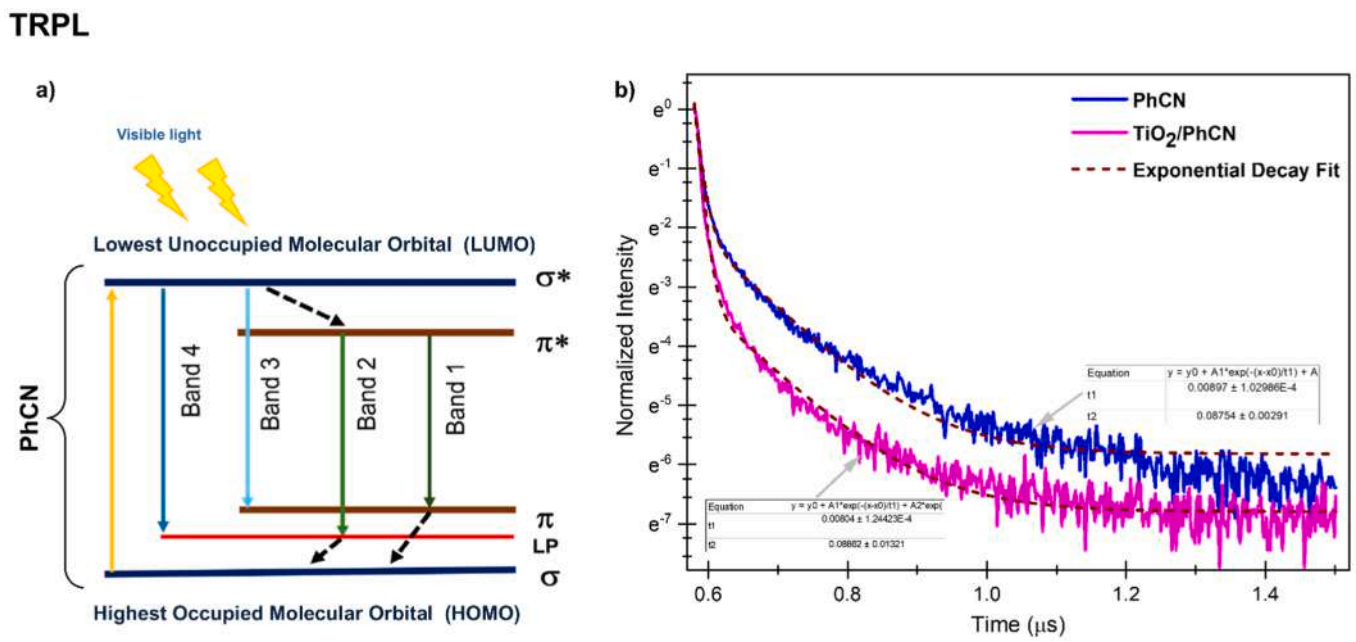

Fig. 9. a) Electronic transitions contributing to the PL spectra in PhCN.,b)Time -resolved photoluminescence measured with 410 nm excitation for the samples PhCN and the hybrid TiO_2/PhCN. The PL decay is fitted as a two-component exponential decay function.

relationship–

$$\frac{1}{\tau_i} = \frac{1}{\tau_R} + \frac{1}{\tau_{NR}} = \gamma_R + \gamma_{NR}$$

By this relationship, a slower decay in the hybrid obtained by the TRPL measurement (τ_i), and a high probability of radiative recombination in the hybrid from the PL measurements (γ_R), we can deduce that the hybridization of PhCN with TiO_2 introduced new non-radiative decay channels compared to pristine PhCN. This higher probability of non-radiative recombination is an indication of a charge transfer from PhCN to the TiO_2 which is ideal for visible-light photocatalytic activity.

3.10. Photocatalytic dye degradation

To verify the photocatalytic ability of the generated hybrid TiO_2/PhCN and assess whether it has a visible-light response, we conducted degradation experiments with organic dye pollutants Methylene blue (MB), Methyl orange (MO) and RhodamineB (RhB). MB is a cationic dye (forms majorly cations when dissolved in water), MO is anionic in nature and RhB is zwitterionic. (Elnagar et al., 2026; Yaacob et al., 2026; Walhout et al., 2022) All three of them are commonly used in industry colorings and are common water pollutants. Before proceeding with the photocatalytic degradation experiments with the hybrid, control experiments investigating the natural degradation of the dyes under the white LED lamp were performed as shown in Fig. 10b,d,f. The MB dye showed the absorption peak at 664 nm with a degradation of 16.7% under white light (Fig. 10b). On the other hand, MO dye showed a negligible degradation of 4% under the LED lamp (Fig. 10d) where the absorption peak was at 464 nm. The RhB dye showed its characteristic absorption peak at 554 nm and did not show any change in the concentration even after 4 h of illumination under the white LED lamp (Fig. 10f). The control experiments with the white light show how the light source affects the dye solutions. The photocatalytic dye degradation experiments were conducted under the illumination from the same white LED source. 50 ml of 0.2 mM dye solutions were used for all the experiments as described in the methods section. The TiO_2/PhCN photocatalyst concentration was 1 g/l in the dye solutions. Before the light was switched on, the dye solutions and the photocatalyst powder were left to dissolve in the dark for 30mins to achieve the adsorption-desorption equilibrium.

The MB dye showed a drastic change in the absorption peak at 292 nm within 30mins in the dark with the hybrid TiO_2/PhCN as observable in Fig. 10a. This peak is related to the electronic transitions from the localized chromophore segments while the peak at 664 nm is the monomeric transition. (Dinh et al., 2019) The intensity of the peak at 292 nm increases when the mixture is kept in the dark, showing a high level of molecular interaction of MB with the hybrid photocatalyst. Meanwhile the peak at 664 nm does not shift or show significant change in intensity which suggests that the overall concentration of Mb dye in the solution stays the same even after 4 h of illumination.

MO dye in Fig. 10c showed a high adsorption on the surface of the photocatalyst in the first 30mins in the dark through the decrease in the characteristic peak intensity. A red-shift was also observed from 464 nm to 491 nm for the MO peak which is an indication of an acidic pH of the solution. (Xin et al., 2012) When illuminated, successful degradation of the dye was observed in 4 h where the appearance of new peaks indicated formation of new species through the photocatalytic reactions. The control experiment in Fig. 10d ensures that the degradation observed is due to the presence of the photocatalyst powder. The rate of degradation of MO dye during visible-light illumination was calculated using the pseudo-first order rate equation:

$$ln\left(\frac{C}{C_0}\right) = -kt$$

and was found to be $0.665 \times 10^{-2}\,min^{-1}$. It must be noted that the major removal of MO dye already happened in the dark through the process of adsorption on the surface of the photocatalyst and the rate shown above is the rate of degradation of the remaining amount of the dye under illumination of white light due to the photocatalytic reaction. This 4 h illumination time can be regarded as photocatalysis because Fig. 10d does not show significant dye degradation during exposure under the same light source. Hence, the degradation in Fig. 10c can be attributed to the presence of the hybrid photocatalyst TiO_2/PhCN.

For the RhB dye degradation, similar experiment was performed and it was observed that the hybrid photocatalyst did not adsorb this dye as much as MO in the dark (Fig. 10e). When visible light was incident on the system, RhB rapidly degradaded within 3 h. The rate of the RhB

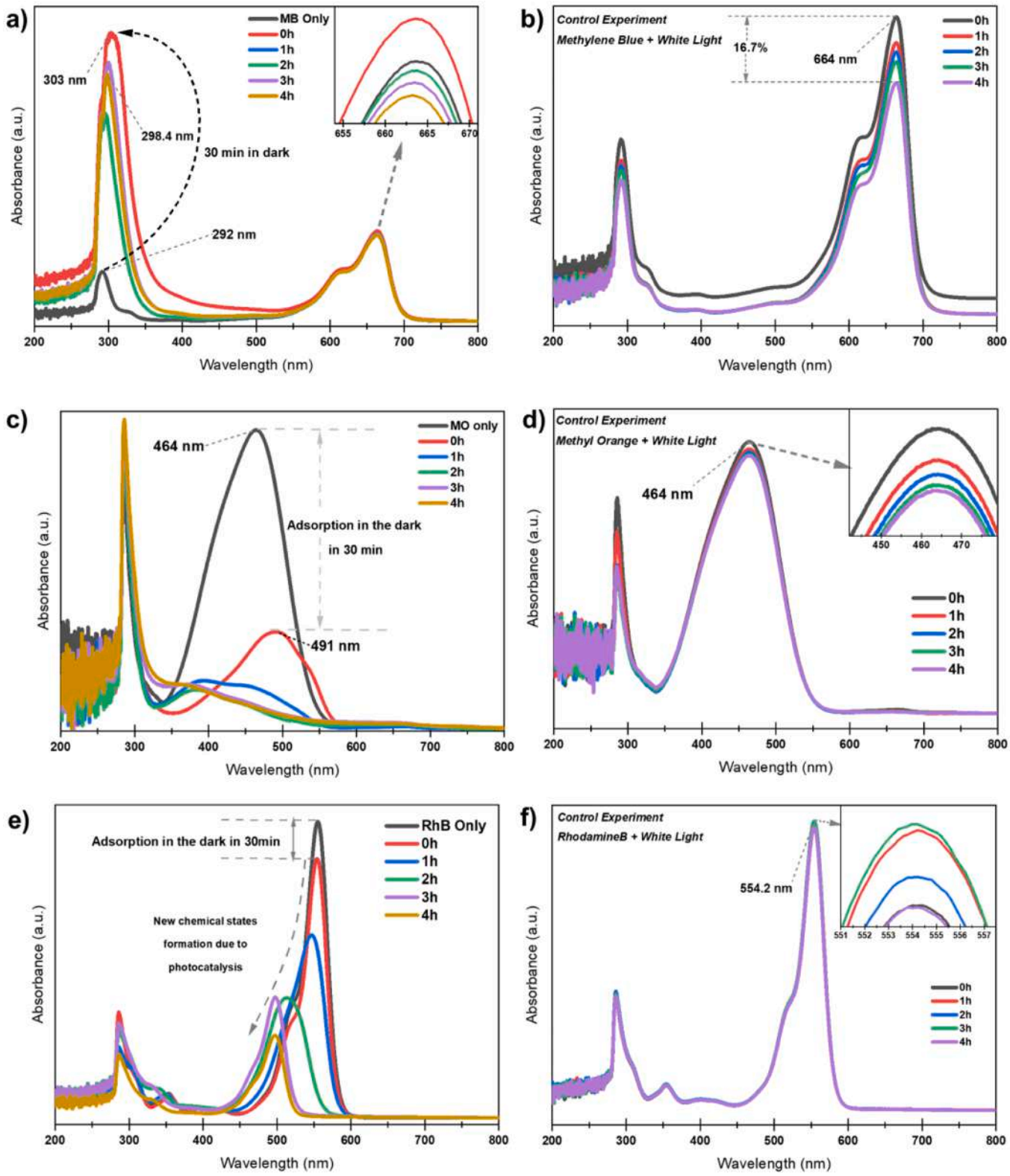

Fig. 10. a) Methylene blue degradation by TiO_2/PhCN hybrid under white light irradiation, b) Methylene Blue dye degradation under white light irradiation, c) Methyl Orange degradation by TiO_2/PhCN hybrid under white light irradiation, d) Methyl Orange dye degradation under white light irradiation, a) Rhodamine B degradation by TiO_2/PhCN hybrid under white light irradiation, b) Rhodamine B dye degradation under white light irradiation.

removal reaction was found to be 2.34×10^{-2} min^{-1} which is much higher than MO removal reaction. Fig. 10e shows the appearance of absorption peaks at different wavelengths than the characteristic 554 nm of RhB which shows the change in its chemical composition with time. Taking into account the control experiment depicted in Fig. 10f, it can be concluded that the hybrid photocatalyst TiO_2/PhCN works very well for the degradation of RhB dye under visible-light illumination, where the light alone does not play any role in RhB degradation.

The difference in the interaction of TiO_2/PhCN with MB, MO and RhB provides an important insight to the surface properties of the powder photocatalyst. For a succesful heterogeneous phtotocatalytic dye degradation, the first step is the adsorption of the dye molecules on the surface of the solid photocatalytic particles. (Hu et al., 2011) This adherence of the dye molecules to the photocatalyst is crucial, as the redox reaction pertaining to the photocatalysis happens on the surface of the photocatalytic particles. When the dyes are dissolved in water, they tend to form ions depending on their chemical composition. The MB dye forms cations, the MO dye forms anions and, the RhB dye forms zwitterions (both poistive and a negative charged ions). When the photocatalyst is added to water and a colloid is formed, the colloidal particles (the TiO_2/PhCN particles) also depict a surface charge due to the protonation or deprotonation of surface ionizable groups. (Ong et al., 2020) From the observations depicted by the dye degrdadation experiments, the TiO_2/PhCN can be assigned to have a positive surface charge which repels the cationic MB dye and avoids any adsorption which ultimately does not yield the photocatalytic degradation. This positive surface charge attracts the negatively charged MO dye very strongly, leading to a strong adsorption in the dark. On the other hand, the electrostatic balance is maintained for the RhB dye pertaining to its zwitterionic nature and the photocatalyst particles are able to interact with the RhB molecules. This balance leads to an optimal level of adsorption of the dye molecules on the surface of the photocatalyst without quenching the catalytic active sites. The surface charge of TiO_2/PhCN particles in acqueous media was also verified by the pH information from the interaction of the hybrid with the MO dye and zeta potential data. The red shift in Fig. 10c indicated the acqueous solution to be acidic, this can also be indicated by the colour change of MO dye when TiO_2/PhCN was added to it. Figure S4 shows the colour change from yellow (MO dye alone) to orange when the hybrid photocatalyst was added to the solution. Since MO acts as a good pH indicator, this orange colour shows the pH of the solution to be <7. This information indicated that when TiO_2/PhCN is added in water, the medium has pH<7. The pH of the medium and the solvent act as the deciding factors for the protonation/deprotonation of the colloidal particles in it. (Ong et al., 2020) The literature reports that TiO_2 anatase exhibits a positive surface charge for an acidic pH. (Holmberg et al., 2013) We conducted zeta potential measurement for PhCN,as shown in Figure S5, and it was found that it too exhibits a positive surface charge in pH<7.0. From the XRD, FTIR, TEM and UV–Vis data, it is clear that the hybrid TiO_2/PhCN does not form new chemical structures but simply form an interface between the two components which maintain their pristine characteristics. The gradient core-shell structure of the hybrid indicates a shell composed majorly of TiO_2 with certain areas composed of PhCN. As both the entities on the surface of the hybrid exhibit positive surface charge in acidic acqueous medium, it is safe to say that the hybrid follows the same. Hence, the TiO_2/PhCN demonstrates a positive surface charge for the dye removal tests.

To verify the photocatalytic reaction, another control test was performed in the dark by mixing the RhB solution with the hybrid photocatalyst powder for 4 h (Fig. 11a). It was observed that the RhB did not show any further adsorption on the surface of TiO_2/PhCN even in 4 h. Therefore the degradation of RhB by TiO_2/PhCN does not posses any adsorption features and the removal is solely reliant on photocatalysis. Another reference test with only the anatase TiO_2 was also conducted to check its photocatalytic efficiency under the same LED light (Fig. 9a) and it was observed that in 4 h, TiO_2 was not able to degrade even 5% of the dye. Hence, the hybrid TiO_2/PhCN could utilize the visibe light spectrum successfully which could not be utilised by TiO_2 for the same photocatalytic reaction. Fig. 11b shows the recycle tests done for the RhB degradation using the TiO_2/PhCN hybrid. The hybrid showed a successful degradation of 0.02 mM RhB dye within 3 h for 3 back to back cycles, where the first cycle demonstrated a 100% degradation, the 2nd cycle a 99% degrdation and the 3rd cycle a 98% degradation. This provides a nod for the utilization of this hybrid photocatalyst for the potential replacement of TiO_2 in other applications like photocatalytic paints or cements which demand for the longevity of the photocatalyst. The successful interaction with the organic RhB and MO dye molecules indicate a potential use in photocatalytic removal of gaseous organic pollutants like the PAHs and carbonaceous matter under white LED light.

3.11. *Photocatalytic coatings*

The dye degradation results depict that the hybrid is active in the oxidation of organic molecules thus, holding promise in organic pollutants degradation in the air too. The degradation of carbonaceous and organic compounds present in the air as pollutants using TiO_2/PhCN coatings was studied through a combined approach utilizing reflectivity, colorimetric and Raman analyses at various stages of the photocatalysis. The surface sensitive photocatalytic processes occurring on coated substrates often result in the gradual removal of deposited organic species, such as cigarette smoke residues, which manifest as measurable changes in optical properties. Reflectance spectroscopy provides a direct quantification of surface cleanliness by monitoring the recovery of light reflectance following pollutant deposition. A decrease in reflectance is typically associated with the accumulation of light-absorbing dark

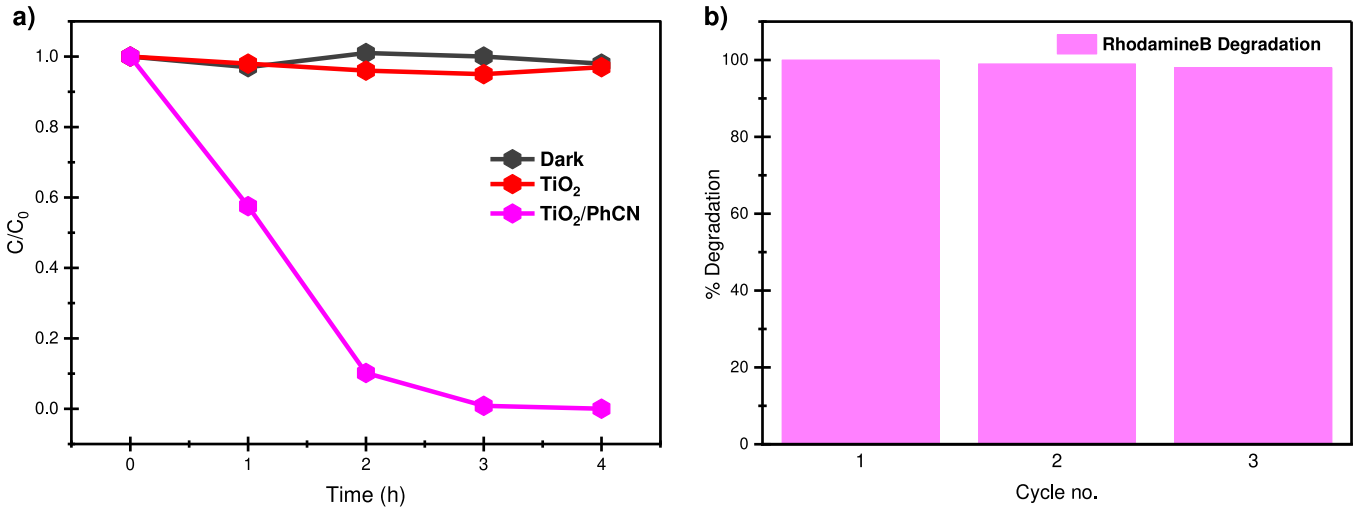

Fig. 11. a) Control test in the dark and reference test with TiO_2 in comparison with RhB degradation test under visible light with TiO_2/PhCN. b)% degradation of RhB dye by the TiO_2/PhCN hybrid under visible light in different in three cycles.

coloured carbonaceous species, whereas its recovery under illumination indicates photocatalytic degradation and removal of these deposits. Complementarily, colorimetric analysis, particularly in the CIE L*a*b* colour space, enables the quantification of perceptible changes in surface appearance, which is critical for coatings intended for indoor applications. Parameters such as lightness (L*) and total colour difference (ΔE) provide sensitive indicators of fouling and subsequent self-cleaning behaviour. Both these techniques are of non-destructive nature and easy to implement, and are complementary, where visual cleanliness and optical performance are key functional requirements. The self-cleaning process of the coatings through the phenomenon of photocatalysis is surface sensitive as the coatings also adsorb the carbonaceous matter on the surface which when interacts with the photocatalyst particle, degrades into other products. As this is a surface phenomenon, the surface area of the coatings was kept the same for all the tests.

The TiO_2/PhCN photocatalyst was tested for the removal of carbonaceous matter under only visible light by utilising the same LED source as used for the dye degradation experiments. As one of the consistent and popular indoor smoke sources is cigarette smoking, it was used as the model pollutant. Fig. 12a shows the reflectance measurements for this test. The sample T_x which only has the hybrid TiO_2/PhCN photocatalyst, shows low reflectance for the UV light but as slowly increasing reflectance of the visible light which corroborates with the UV–Vis absorption spectra of the same sample in powder form shown in Fig. 7a. As the coating was subjected to fumigation, there was a visible layer of particulate matter formed on top of the coating in C_T_0 which is darker

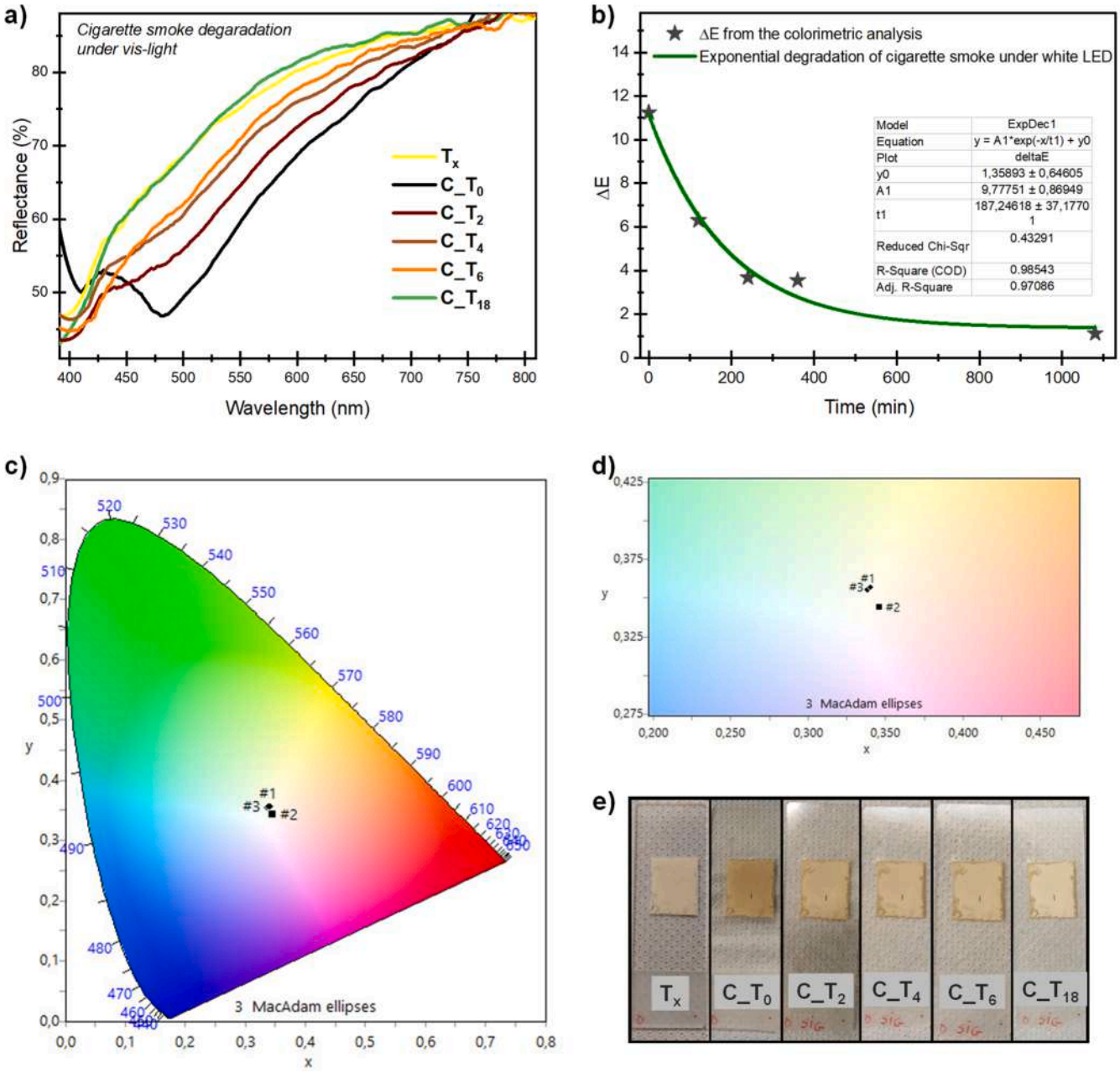

Fig. 12. a) Reflectance measurements for the coatings undergone visible-light degradation of cigarette smoke carbonaceous matter, b) Total colour difference ΔE calculated through the colorimetric analysis for the coatings undergone visible-light degradation of cigarette smoke, c) The Color diagram of coating undergone cigarette smoke. The graph shows the three main color points for the sample: 1 = initial color of the sample, T_x, 2 = color of the sample after the smoking process, C_T_0 3) color of the sample after 18 h of exposure to light, C_T_{18}. d) Zoomed in colour diagram shown in 9c, e) Photographic images of all the coating samples studied.

in colour (Fig. 12e). The reflectance data of the samples C_T_2, C_T_4, C_T_6 in Fig. 12a, unravels a gradual deterioration of the cigarette smoke residues, where the reflectance values start to increase for the incident light as more and more of the particulate matter was lost. The sample C_T_{18} showed the reflectance arc like the initial clean sample T_x indicating a successful recovery. This is also visible by the colour change to the naked eye as evident in the Fig. 12e.

The colorimetric study yielded an accurate quantization of this colour change phenomenon, which is depicted in Fig. 12b,c,d. CIE L*,a*, b* coordinates were utilized to calculate the total color variation ΔE by using the method described in Section 2.7. Each data point in Fig. 12b shows the colour variation of the polluted sample at different illumination times compared to the initially clean sample.The colorimetric cleaning efficiency for this case was found to be 90.05% in 18 h of LED illumination. Where the calculations were made as follows:

$$\eta_{colour}(\%) = \frac{\Delta E_{T_0-T_{18}}}{\Delta E_{T_X-T_0}} \times 100$$

Where $\eta_{colour} \approx 100\%$ means full optical recovery. Fig. 12b depicted the exponential decay of the carbonaceous matter deposited on top of the coating. The first order exponential decay fitting using the equation:

$$y = A\, e^{\left(-\frac{x}{t}\right)} + y_0$$

to obtain the time constant as (187± 37) min which indicates the time

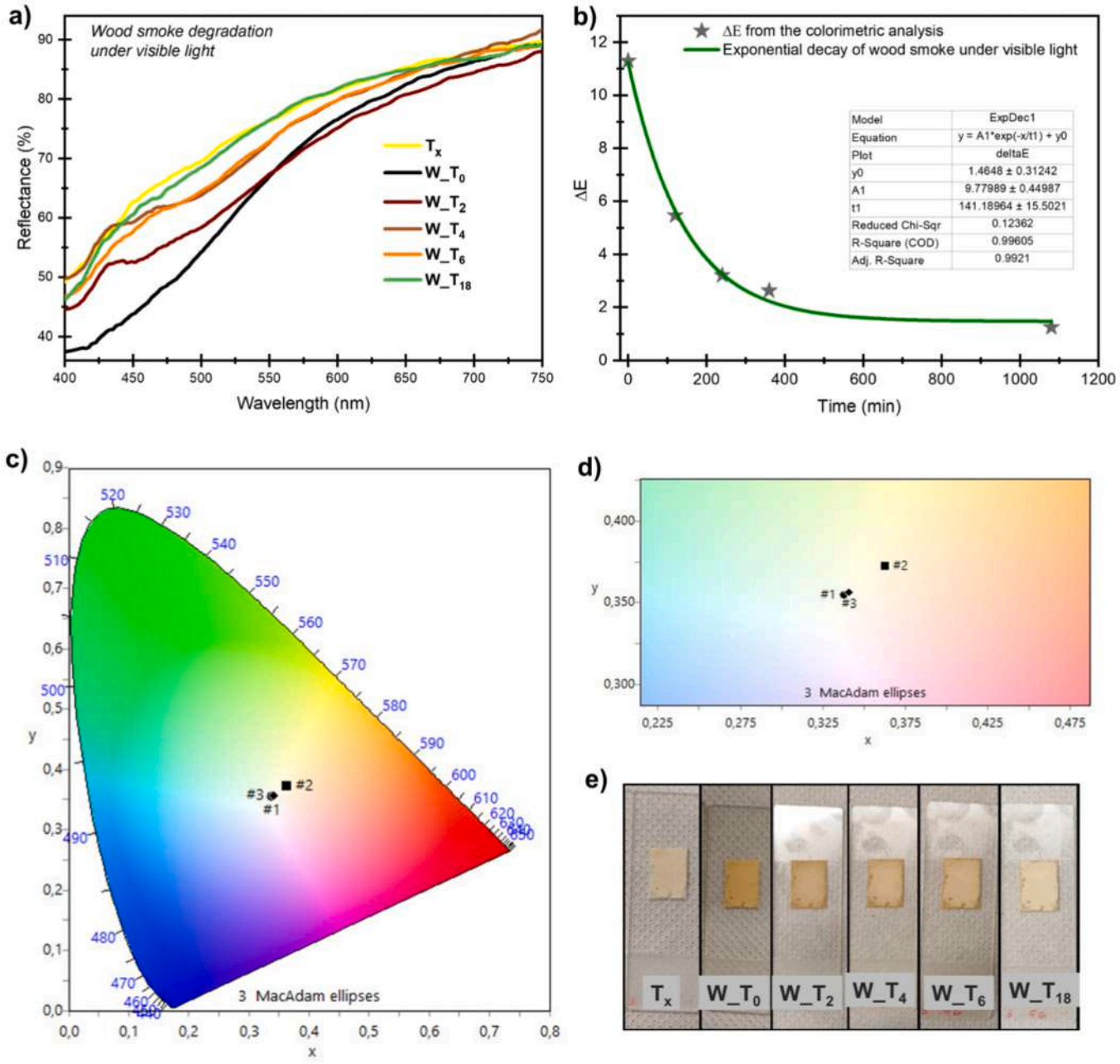

Fig. 13. a) Reflectance measurements for the coatings undergone visible-light degradation of wood-burning smoke carbonaceous matter, b) Total colour difference ΔE calculated through the colorimetric analysis for the coatings undergone visible-light degradation of wood-burning smoke, c) The Color diagram of coating undergone wood-burning smoke. The graph shows the three main color points for the sample: 1 = initial color of the sample, T_x, 2 = color of the sample after the smoking process, W_T_0 3) color of the sample after 18 h of exposure to visible light, W_T_{18}. d) Zoomed in colour diagram shown in 9c, e) Photographic images of all the coating samples studied.

taken to achieve 63% of the total photocatalytic process.

For reference, a similar experiment with a TiO_2 coating was also performed, depicted in Figure S6 a,b, where the reflectivity of the TiO_2 coating after cigarette-smoking showed a drop in the reflectance especially in the low wavelength region. When this coating was illuminated under white LED light for 8 h, it did not show self-cleaning characteristics. This process was again repeated in the dark for the smoked TiO_2 coating, and it showed the same reflectivity arc as it showed in 8 h in light. This verified the ineffective photocatalysis by TiO_2 under visible-light irradiation and the necessity of PhCN in the hybrid. We then also performed reference experiments with pristine PhCN coating under the same conditions as shown in Figure S6 c reflectance measurements. The spectra do not show any significant change in the reflectance after smoking for 30 mins. This experiment was repeated three times and identical results were recorded, where only miniscule changes were observed in the DRS spectrum of the PhCN coating after smoking. This is a result of an ineffective adsorption of the soot particles on the surface of the PhCN coating. Therefore, PhCN cannot be regarded as a suitable material for self-cleaning purpose as it does not interact ideally with the carbonaceous particles present in the cigarette smoke. The hybridization of PhCN with TiO_2 changes the surface chemistry in such a way that favors soot deposition and subsequent photocatalytic action. These experiments establish the need for both the components in the hybrid where TiO_2 enhances the photocatalytic ability of PhCN without acting as the primary photocatalyst under visible light, and PhCN acts as the primary photocatalytic material and provides visible-light activity. TiO_2/PhCN performs as an effective visible-light active photocatalytic coating material superior to TiO_2 for indoor pollution from cigarette smoke residues.

For the successful utilization of a material as a photocatalytic coating for indoor pollutant removal, it should be effective for different pollution sources. Therefore, we did similar experiments under visible-light illumination and used wood-burning smoke as the pollution source. Fig. 13a shows the reflectance spectra of the samples used in this experiment. The polluted sample W_T_0 showed a decrease in the reflectance than the pure and clean sample especially in the UV region. When compared with the C_T_0 sample's reflectance in Fig. 13a, the polluted sample from the wood smoke appears to be different in optical characteristics than the one smoked from cigarettes. This indicates that the nature and chemistry of the pollutants/soot is different for the two cases. When visible light was incident on the polluted W_T_0, it started to go back to its original reflectance spectrum. The Fig. 13b depicts the colorimetric data for the degradation of the pollutants related to the wood-burning smoke on the surface of the coatings. The exponential decay shows the time constant at 141±15 min and the degradation of 89% of the particulate matter in 18 h.

The comprehensive analysis of reflectance spectra and colorimetry provides a nuanced understanding of the temporal evolution of the hybrid TiO_2/PhCN under specific environmental conditions. Table 1 summarizes the quantifications obtained by the above two experiments. The prepared coatings have comparable efficiencies for cigarette related and wood related smokes. By capturing the intricate interplay between light exposure and degradation dynamics, these findings not only contribute to the comprehension of material behavior but also offer valuable insights for potential applications in areas where controlled degradation is a desirable outcome.

Table 1
The quantization related to smoke related pollutant degradation on top of the TiO_2/PhCN coatings for different experiments and their comparison.

S. No	Case	% Self-cleaning in 6h	Rate of pollutant removal	Time required to degrade 63% of the pollutants
1	Cigarette smoke under LED	68.5	5% h^{-1}	187 min
2	Wood smoke under LED	76.8	5% h^{-1}	141 min

Starting from the reflectance spectra of the sample measured at various moments during its exposure to LED light, it was possible to calculate the color coordinates of the sample. Using these coordinates, ΔE was calculated, representing the distance in the CIE L*ab* color space between the color coordinates of the sample before the smoking process and its coordinates at different stages of the experimental procedure. This analysis reinforces the results obtained from previous measurements on the material's contaminant degradation capabilities, illustrating how the color difference between the initial state and intermediate states progressively decreases with the exposure time to light. The Tables S2 and S3 provide the colour coordinates related to the colorimetric analyses shown in Fig. 12b and 13b respectively.

This comprehensive evaluation of optical character not only highlights the dynamic nature of degradation mechanisms but also emphasizes the adaptability of the TiO_2/PhCN hybrid system in addressing diverse pollutants. The observed distinctiveness in reflectance spectra between different smoke sources further accentuates the system's capability to tailor its response based on the specific composition of the encountered pollutants, showcasing its potential utility in targeted pollution remediation applications for indoors as well as outdoor coatings and paints.

To deepen the study on the degradation of carbonaceous residues derived from cigarette smoking on the coatings, a study was conducted using the non-destructive technique of Raman spectroscopy. Cigarette smoke contains PAHs, amorphous carbon, soot and oxygenated organics. Raman spectroscopy can reveal the graphitic carbon D and G bands from the soot which appear at 1350 cm^{-1} and 1590 cm^{-1} respectively. (Li et al., 2025) By investigating these bands, one could qualitatively and quantitatively analyze the photocatalytic degradation of the carbon soot on the TiO_2/PhCN coatings. A preliminary measurement was taken on the clean sample, which served as a reference for subsequent measurements. The sample was then subjected to cigarette smoke for 30 min, followed by another measurement. Subsequently, the same visible-light irradiation was applied, studying degradation at certain time intervals. Fig. 14a depicts the Raman spectra of all the samples normalised to the intensity of the graphitic G band found at 1596 cm^{-1}. Raman measurements were also conducted on a clean sample not exposed to irradiation to confirm that there was no carbonaceous residues in the air and its bands did not grow over time (Figure S7). Graphitic D and G bands were considered as reference points for degradation, and the observed variations over time followed an exponential decay (Figure S8a), consistent with previous colorimetric analyses. Figure S8a, obtained from the ratio of D to G bands, illustrates the degradation of carbonaceous residues over time. In this case, an exponential function was employed to study the degradation timelines, revealing a time constant of approximately (73±14) minutes to reach 63% of the soot degradation. This time constant was significantly shorter than that observed through color variation analyses because this value is only related to the graphitic content deposited on the surface of the coating due to the cigarette smoke. For colorimetric analysis, the overall discoloration of the material is studied, which can be due to a number of carbonaceous components or chemical complexes in addition to the amorphous graphitic carbon. This also signifies the faster efficiency of the TiO_2/PhCN hybrid in removing amorphous graphitic phases resulting from airborne soot. The Raman measurements focus on a specific surface effect, considering three measurements at different points for each acquisition time and then averaging them. It is crucial to emphasize why the degradation follows an exponential, non-linear pattern. Initially, degradation is rapid due to a higher concentration of carbon soot, which subsequently decreases, leading to a slower process. This degradation process is evident from the decrease in the intensity of the D band w.r.t. the G band in Fig. 14a.

To finally test the reusability of the TiO_2/PhCN coatings under visible-light illumination and attest its durability over time to be applied

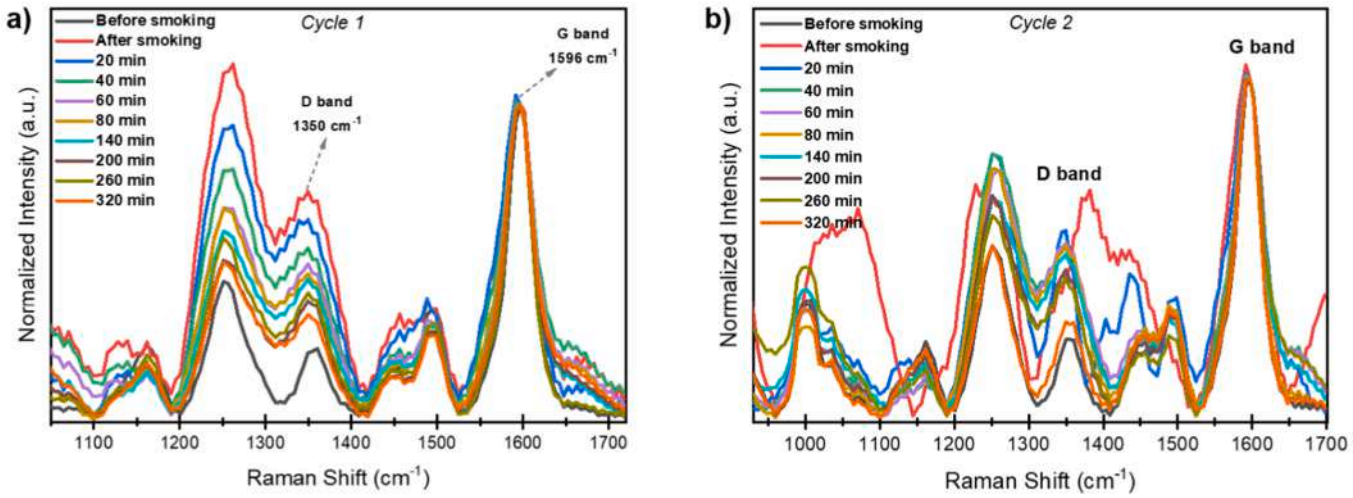

Fig. 14. a) Raman spectra of the TiO_2/PhCN coated samples undergone cigarette smoking and subsequent irradiation under the white light LED. The peaks are normalized to the G band intensity. b) Recycle test of the previously photo- cleaned sample in Fig. 12a.

for real life scenarios, another cycle of photocatalytic cigarette smoke degradation test was monitored with Raman spectroscopy. This time the cleaned sample achieved at the end of cycle 1 was again smoked and then illuminated under white LED. Fig. 14b shows the normalized Raman spectra of the samples' surfaces demonstrate a successful degradation of the carbon soot in this cycle2 while gradually achieving the same spectrum as the reference sample. When the intensities were analyzed with exponential fitting (Figure S8b), it was observed that the time constant came out to be approximately 296 ± 86 min which is much higher than the value observed in cycle 1. Therefore, the self-cleaning process appears to be slower for the second cycle for a 320 min observation time. This suggests a probable deactivation of the hybrid photocatalytic coating which reduces the rate of photocatalytic self-cleaning process. This drop in the efficiency of the photocatalytic coating can be due to a partial surface deactivation caused by residual soot-derived intermediates and changes in surface chemistry after the first cycle.

It must be noted that the experiments with Raman analyses were performed for 320 min (5.33 h), while reflectivity measurements were done for 18 h. Therefore, it is expected for the coating to have a percentage of carbonaceous matter deposited on it even after the first cycle depicted in Fig. 14a. This remaining carbonaceous deposit provides a setback for the second cycle in Fig. 14b by making a layer on top of the coating reducing the visible-light absorption. These residual particles may form interconnected conductive carbon domains across the surface with the graphitic PhCN which in turn could alter the local electrical properties by facilitating electron transport and trapping photo-generated charges, hence the deactivation. If continued for more cycles, this buildup could block more active catalytic sites and shield incident light and can therefore reduce photocatalytic efficiency over time while also changing the coating's surface charge distribution and adsorption behavior towards incoming pollutants. Additionally, the presence of different charged species in the smoke can also neutralize positive/negative catalytic sites of the photocatalyst. Over time, the coating's chemical and electrostatic behaviour can change dramatically which tends to alter the photocatalytic self-cleaning efficiency.

However, the removal of carbonaceous soot on the surface of the coatings was possible even at the second cycle which is evident from the I_{1350}/I_{1596} ratio of the final sample coinciding with the reference sample value. This demonstrates that the TiO_2/PhCN photocatalytic coating retains its soot-removal capability even after repeated exposure within short time intervals, thereby maintaining its self-cleaning performance. For a more realistic and practical assessment of the coating durability, future studies should investigate the influence of varying coating areas, deposition thicknesses, and prolonged exposure periods under multiple cycles of cigarette smoke deposition. However, such investigations are beyond the scope of the present work.

3.12. *Indoor pollution control by TiO_2/PhCN*

As mentioned in the introduction section, the smokes from cigarette and wood-burning contain a large number of air pollutants which contribute to the wear and tear of the building materials and surfaces, however, the content of these two types of smokes are different. Smoke from a burning cigarette contains PAHs, aromatic hydrocarbons, carbonyls (aldehydes/ketones), nicotine, phenols, metals, nitrosamines, and abundant organic and elemental carbon, along with PM which is dominated by organic carbon, with ions (Cl^-, SO_4^{2-}, NH_4^+, NO_3^-) and metals (V, As, Zn, Cd, etc.). (Soleimani et al., 2022; Vu et al., 2015; Zhao et al., 2023) The most carcinogenic component– cigarette tar, contains benzene, acrylamide, and nitriles, along with heavy metals and stable semiquinone radicals. (Xiao et al., 2025) On the other hand, smoke from the burning of wood is formed from pyrolysis of cellulose/hemicellulose and lignin, producing phenols, organic acids, carbonyls, PAHs, anhydrosugars (e.g., levoglucosan), and many VOCs. (Desvita et al., 2025; Chomanee et al., 2009) This smoke also includes CO, CH_4, NOx, and diverse organic aerosol components. (Wheeler et al., 2014) These aerosol particles rarely remain perfectly electrically neutral because they continuously interact with ions, radiation, water vapor, surfaces, and other particles in the atmosphere. The magnitude and polarity of the charge depend on the particle composition, size, source, humidity, and surrounding environment. (Nanni et al., 1990) Out of the above-mentioned chemical, PAHs, phenols, and tarry organic carbon accumulate on surfaces as grime, creating an unclean appearance. (Chan et al., 2025) Wood smoke notably increases PAH levels, forming a persistent dark layer, which can also alter paint binders and pigments (e.g., lead oxides, carbonates, and carboxylates), leading to discoloration and degradation. (Dolske, 1995; Chen et al., 2011) This work aimed to provide a photocatalytic self-cleaning alternative to the pollution of indoor surfaces by the soot particles and PAHs from the smokes of cigarette and wood.

For an effective photocatalytic process to take place, the adsorption of the pollutant molecules is the foremost important step. (Mo et al., 2009) Successful adsorption of soot/PAHs onto the photocatalyst is mainly controlled by surface area and porosity, hydrophobicity and site-specific interactions (OH groups, oxygen vacancies, metal centers), and by environmental conditions such as pH, humidity, and co-foulants that compete for or block surface sites. (Stefanakis et al., 2021; Lee and

Choi, 2002; Li and Li, 2021; Kovalevskiy et al., 2018) From the XRD, SEM, Raman and TEM analyses, we can conclude that the surface area of the hybrid is higher than the surface of pristine TiO_2 owing to the smaller size of the TiO_2 nanocrystallites in the hybrid. This enhancement in the surface area enables a high adsorption of the soot particles. Furthermore, PhCN is reported to be non-porous with a low surface area of 5.9 m^2/g, which can be the reason why the soot particles were not adsorbed on the surface of the PhCN coatings in the control tests in Figure S6c. (Hazra et al., 2025) On the other hand, isolated surface –OH groups on TiO_2 are key adsorption sites for organics. (Lee and Choi, 2002) Oxygen vacancies on TiO_2 also enhance the interaction with the pollutants and enhance adsorption. The presence of TiO_2 as the outer shell in the core-shell structure of the TiO_2/PhCN hybrid led to a higher adsorption of the soot particles/PAHs on its surface. The surface of a photocatalyst would highly adsorb the molecules with the opposite surface charge. However, extreme exposure to smoke will quench the catalytic sites and shield them from the incident light, which will fail the next step of photodegradation. This is the reason why the exposure time was kept at 30 mins for our experiments as 40 mins exposure did not show any photodegradation.

In terms of surface charge, PAHs do not inherently depict a positive or negative surface charge but the aerosol particles carrying PAHs determine the net charge behavior. (Shimazu, 2016) From our photocatalytic tests it is evident that the hybrid TiO_2/PhCN coating was able to tackle the pollutants from both these sources and prevent the discolouration effect which is mainly from PAHs, therefore the hybrid must have exhibited an ideal surface charge in the conditions of the experiment. In fact, TiO_2/PhCN photocatalytic coating in air can exhibit a dynamic surface charge which is subject to change with UV illumination, humidity, oxygen adsorption and contact molecules. (Holmberg et al., 2013) A positive zeta potential in water suggests protonated or positively biased surface chemistry, but it does not directly prove a positive net charge in air. (Ong et al., 2020) When differently charged-particles from wood-burning and cigarette would contact the TiO_2/PhCN coating, electrostatic attraction (for unlike charges) would lead to a higher particulate matter deposition while, repulsion (for alike charges) would reduce particle deposition and photocatalytic efficiency. Overall, the smoke itself could progressively alter the coating's surface charge and reactivity by neutralizing surface sites and insulating the layer with time. (Nanni et al., 1990)

The next step, after the adsorption of the pollutants on the surface of the photocatalyst, is the absorption of the incident visible light by the PhCN component of the hybrid (as suggested by DRS measurements) to generate charge carriers (e^-/h^+). The recombination of these charge carriers is prevented by a charge transfer to TiO_2 component in the hybrid (as suggested by TRPL). Then, the electrons on the surface of TiO_2 and the holes on PhCN, react with adsorbed water and oxygen to form reactive oxidation species (·OH, O_2^-,$^1O_2$). Our previous work has proven the generation of ROS by the hybrid TiO_2/PhCN. (Hazra et al., 2025) The generated ROS then react with the adsorbed pollutant PAHs.

PAHs are multi-ring aromatic hydrocarbons with fused benzene rings, the chemical structures are shown in Figure S9. (Vu et al., 2015) The presence of aromatic rings and π-systems makes them susceptible to electrophilic attack and ring-opening by ROS (·OH, $\cdot O_2^-$, $^1O_2$). (Li and Li, 2021) This kind of degradation mechanism has also been prevalent in photocatalytic dye degradation, where the large water-soluble dyes with extended π-conjugation (chromophores) and heteroatoms (N, S) give strong visible absorption and clear colour changes during degradation as shown in Fig. 10. This degradation mechanism is dependent on the generation of reactive oxygen species (ROS) OH^-, O_2^-, sometimes $^1O_2$ and h^+, which attack organic molecules and mineralize them to CO_2, H_2O, and inorganic ions. (Li and Li, 2021; Elattar et al., 2026; Li and Meng, 2020) From our previous work, it can be stated that the hybrid TiO_2/PhCN generates the ROS for the degradation of RhB dye which then can be extended to the degradation of PAHs from the different smokes studied in this work. (Hazra et al., 2025) It was established that this hybrid photocatalyst is rich in generating h^+, OH^- and O_2^- radicals which are essential for the mineralization of organic pollutants in the smoke. (Hazra et al., 2025; Kovalevskiy et al., 2018) Therefore, following steps could be proposed for the photocatalytic degradation of smoke by TiO_2/PhCN: (Mo et al., 2009; Yola et al., 2014; Yi et al., 2024; Liu and Lin, 2019)

$TiO_2/PhCN + h\nu \rightarrow e^- + h^+$ (TiO_2/PhCN)

$e^- + O_2$ (environment) → $\bullet O_2^-$

$h^+ + H_2O \rightarrow \bullet OH$

$H_2O + \bullet O_2^- \rightarrow 2\ \bullet OH$

$h^+/\bullet O_2^-/\bullet OH$ + aromatic rings → stepwise dealkylation → ring hydroxylation

ring opening → short-chain acids → CO_2, H_2O

Intermediates like catechol, hydroquinone, followed by small acids (oxalic, acetic, formic) are formed before full mineralization of the organic pollutants to form CO_2 and H_2O. (Wang et al., 2021) Fig. 15 illustrates the photocatalytic process leading to the self-cleaning of the TiO_2/PhCN coating from smoke deposits.

Overall, this study presents a cost-effective, earth abundant, environmentally friendly, visible-light active, easily producible, hybrid photocatalytic material TiO_2/PhCN, which can be utilized as a futuristic material for indoor photocatalytic paints and coatings to remove pollutants originating from various types of smoke.

4. Conclusions

In conclusion, this study focused on the characterization and investigation of the inorganic-organic hybrid system TiO_2/PhCN. Specifically, the emphasis was on its capabilities for degrading carbonaceous particulate matter, soot and visible non-volatile pollutants originating from cigarette and wood-burning smoke, through a photocatalytic process under visible-light illumination.

A core-shell structure was found to be exhibited by the hybrid where the core consisted of the carbon nitride and the shell was made of TiO_2. The hybrid demonstrated a smaller size than its components, and hinted at a higher surface area which resulted in better adsorption of pollutant molecules on its surface. The presence of phenyl modified carbon nitride in the hybrid yielded a high visible-light absorption to generate electron-hole pairs where the electrons were transferred to the TiO_2 which reduced the rapid charge carrier recombination in PhCN. The TiO_2/PhCN photocatalyst was tested for the degradation of various organic dye pollutants–methyl orange, methylene blue and rhodamine B, under visible-light illumination. These tests resulted in a MO degradation rate of $0.665 \times 10^{-2}\ min^{-1}$ and a RhB degradation rate of $2.34 \times 10^{-2}\ min^{-1}$ and indicated that the photocatalyst does not interact with MB dye due to its positive surface charge. The control tests and multiple cycles of rhodamineB degradation depicted the long life of the photocatalytic ability of the material and the absence of photocorrosion. Finally, the hybrid was tested as a photocatalytic coating to remove particulate carbonaceous matter originating from cigarettes as well as wood-burning smokes under a simple white LED light. The coatings demonstrated a successful removal of carbonaceous matter through Raman measurements showing an exponential decay in the graphitic content over time. The reflectance and colorimetric analyses demonstrated the high efficiency of TiO_2/PhCN coating in regaining their original colour in a short span of time with an exponential rate. The efficient pollutant removal from the common indoor soot sources (cigarette and wood) establishes the efficacy of this material to tackle various kinds of pollutants. Additionally, the hybrid coatings demonstrated effective soot removal from cigarette smoke when reused. This established the longevity of this material as a photocatalytic coating. By combining the

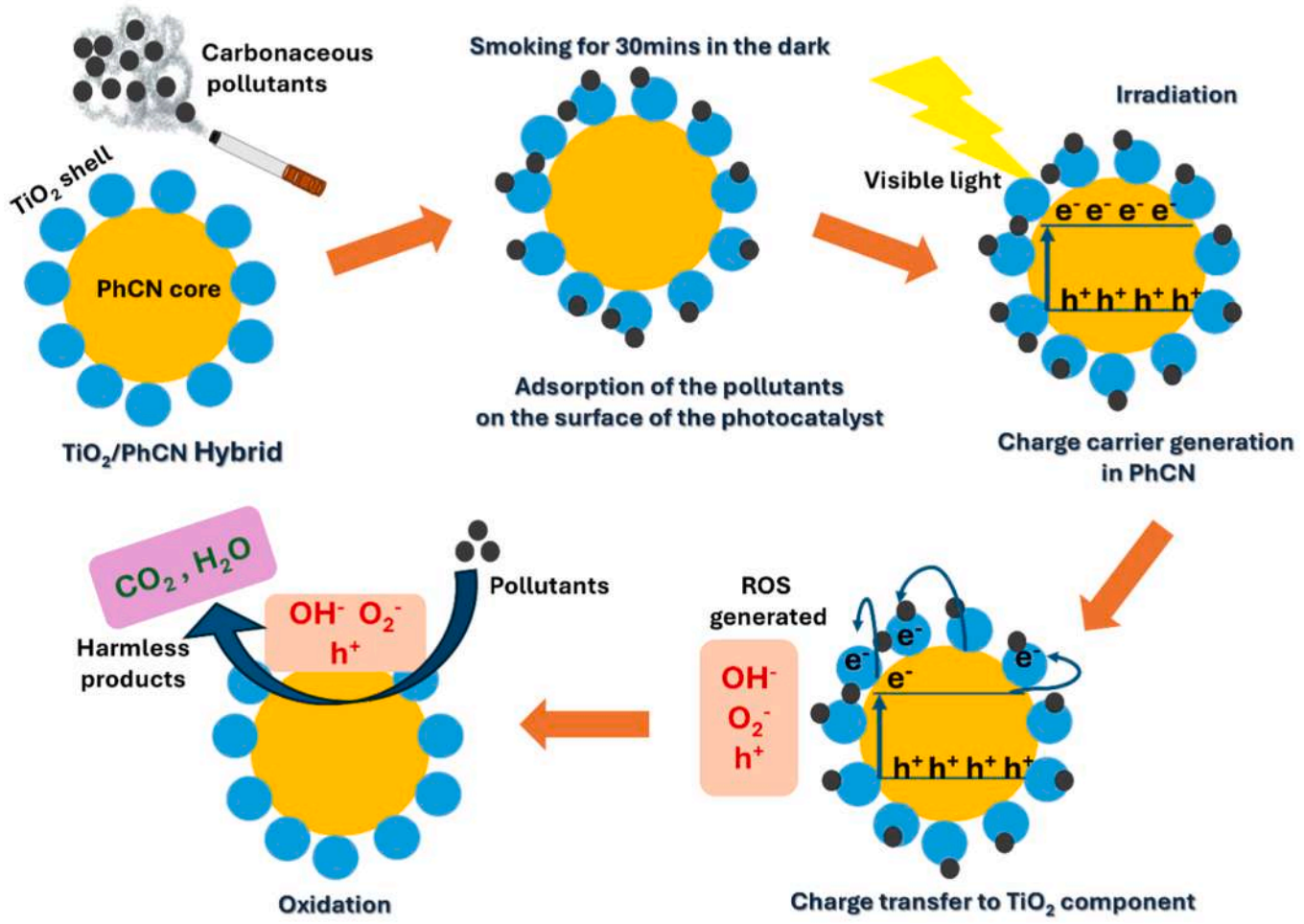

Fig. 15. Schematic illustration of the process of photocatalytic self-cleaning in TiO_2/PhCN from indoor air pollution from smoke.

robustness of TiO_2 with the visible-light sensitivity of phenyl-modified carbon nitride (PhCN), the system overcomes the intrinsic limitations of current photocatalytic paints and coatings. The π-π interactions between phenyl groups of PhCN and the organic pollutant molecules improves the photocatalytic degradation efficiency.

The experiments conducted using various types of contaminants demonstrate that the studied material is highly promising in addressing the issue of indoor pollution as it was highly effective under a simple LED white bulb. Simultaneously, photocatalysis proves to be a "green" technique suitable for various applications in this field. This photocatalytic coating made up of TiO_2/PhCN has future uses in prevention of airborne diseases, conservation of cultural heritage and microclimate control replacing TiO_2 and UV light sources from the scene. The results of this study will pave the way for a new generation of self-cleaning and air-purifying coatings and building materials that operate efficiently under everyday lighting conditions. Ultimately, the successful implementation of such materials, after standardization tests, could contribute to healthier living environments and the broader goal of sustainable urban development.

5. Submission declaration

This article has not been published previously except in the form of an abstract and is not under consideration for publication elsewhere. The article's publication is approved by all authors and by the responsible authorities where the work was carried out. If accepted, the article will not be published elsewhere in the same form, in English or in any other language, including electronically, without the written consent of the copyright-holder.

Funding sources

This research was funded by Fondazione di Sardegna, project FDS2022 "New diagnostic techniques for ancient books restauration and conservation" CUP F73C23001560007. The authors acknowledge support from the University of Cagliari under Open Access funding call for the publication of this work.

CRediT authorship contribution statement

Stefania Porcu: Writing – review & editing, Writing – original draft, Project administration, Methodology, Investigation, Formal analysis, Data curation, Conceptualization. **Moulika Hazra:** Writing – review & editing, Writing – original draft, Visualization, Investigation, Formal analysis, Data curation. **Riccardo Lodo:** Writing – review & editing, Investigation, Formal analysis, Data curation. **Daniele Chiriu:** Writing – review & editing, Supervision, Resources, Project administration, Funding acquisition, Formal analysis, Data curation. **Pier Carlo Ricci:** Writing – review & editing, Visualization, Resources, Project administration, Methodology, Conceptualization.

Declaration of competing interest

The authors declare that they have no known competing financial interests or personal relationships that could have appeared to influence the work reported in this paper.

Supplementary materials

Supplementary material associated with this article can be found, in the online version, at doi:10.1016/j.hazadv.2026.101389.

Data availability

Data will be made available on request.

References

Alsharief, H.H., et al., 2026. Efficient and durable dye-sensitized solar cells using a donor–donor–acceptor organic sensitizer and a conductive polymer–tin selenide–graphene composite electrode. Mater. Chem. Phys. 353, 132151.

Anucha, C.B., Altin, I., Bacaksiz, E., Stathopoulos, V.N., 2022. Titanium dioxide (TiO_2)-based photocatalyst materials activity enhancement for contaminants of emerging concern (CECs) degradation: in the light of modification strategies. Chem. Eng. J. Adv. 10, 100262.

Armaković, S.J., Savanović, M.M., Armaković, S., 2022. Titanium dioxide as the most used photocatalyst for water purification: an overview. Catalysts 13, 26.

Baeza_Romero, M.T., et al., 2022. A review of critical residential buildings parameters and activities when investigating indoor air quality and pollutants. Indoor. Air. 32.

Bagchi, S., et al., 2026. Phenyl-modified carbon nitride nanosheets: enhanced photocatalytic activity via sonication-assisted exfoliation. J. Phys. Chem. Solids 210, 113361.

Bersani, D., Lottici, P.P., Ding, X.-Z., 1998. Phonon confinement effects in the Raman scattering by TiO_2 nanocrystals. Appl. Phys. Lett. 72, 73–75.

Brüninghoff, R., et al., 2019. Time-dependent photoluminescence of nanostructured anatase TiO_2 and the role of bulk and surface processes. J. Phys. Chem. C 123, 26653–26661.

Buonanno, G., Kumar, P., 2025. Household air pollution and health: rethinking indoor exposure in the places we call home. Sci. Rep. 15, 37184.

Cappelletti, G., Ricci, C., Ardizzone, S., Parola, C., Anedda, A., 2005. Aged titania nanoparticles: the simultaneous control of local and long-range properties. J. Phys. Chem. B 109, 4448–4454.

Chan, I., Schneider, S.R., Cheng, A., Styler, S.A., 2025. Wildfire smoke contributions to polycyclic aromatic hydrocarbon loadings in western Canadian urban surface grime. Environ. Sci. Technol. 59, 2745–2753.

Chen, J., Kou, S., Poon, C., 2011. Photocatalytic cement-based materials: comparison of nitrogen oxides and toluene removal potentials and evaluation of self-cleaning performance. Build. Environ. 46, 1827–1833.

Chomanee, J., Tekasakul, S., Tekasakul, P., Furuuchi, M., Otani, Y., 2009. Effects of moisture content and burning period on concentration of smoke particles and particle-bound polycyclic aromatic hydrocarbons from rubber-wood combustion. Aerosol Air Qual. Res. 9, 404–411.

Desvita, H., et al., 2025. Preliminary study on the chemical components of west kalimantan's ubah rukkok wood (<i>santiria griffithii</i>) liquid smoke. J. Ecol. Eng. 26, 343–351.

Dettori, R., et al., 2025. Sustainable photocatalysis with phenyl-modified g-C3N4/TiO2 polymer hybrids: a combined computational and experimental investigation. Polym. (Basel) 17, 1331.

Dinh, V.-P., et al., 2019. Comparison of the uptake of methylene blue on α- and γ-MnO2 nanomaterials. Desalin. Water Treat. 144, 384–392.

Döblinger, M., Lotsch, B.V, Seyfarth, L., Senker, J., Schnick, W., 2008. Structural investigation of a layered carbon nitride polymer by electron diffraction. In: Luysberg, M., Tillmann, K., Weirich, T. (Eds.), EMC 2008 14th European Microscopy Congress 1–5 September 2008, Aachen, Germany. Springer Berlin Heidelberg, Berlin, Heidelberg, pp. 185–186.

Dolske, D.A., 1995. Deposition of atmospheric pollutants to monuments, statues, and buildings. Sci. Total Environ. 167, 15–31.

Dudek, D., Janus, M., 2022. Photoactive cements: a review. Mater. (Basel) 15, 5407.

Durmus, Z., et al., 2025. Effect of the structural features of graphitic carbon nitride (g-C3N4) synthesized via thermal polycondensation of different precursors on the in vitro tumor cell cytotoxicity. Diam. Relat. Mater. 160, 113064.

Elattar, S.M.S., Gebriel, A.A.S., Abdullah, I.D., 2026. Assessing the feasibility of TiO_2 photocatalytic coatings to improve indoor air quality in interactive scaled lecture hall models. J. Eng. Appl. Sci. 73, 25.

Elnagar, R.S., Razek, T.M.A., Nawar, H.A., Mohamed, S.F., 2026. Synthesis and characterization of gamma irradiated magnetic biochar derived from rice straw and grafting with (acrylic acid-co-acrylamide) hydrogel for removing methylene blue dye. J. Hazard. Mater. Adv. 21, 100998.

Ghourichay, S.A., Ricci, P.C., 2026. Advances in carbon based nanomaterials for photocatalytic environmental remediation and solar fuel production. Discov. Mater. 6. https://doi.org/10.1007/s43939-026-00707-2.

Hazra, M., et al., 2025b. 2D-2D PhCN/WS2 exfoliated nanosheets for visible-light hydrogen production: a platinum-free Co-catalyst approach. Carbon N. Y 244, 120678.

Hazra, M., et al., 2025a. Elucidation of a core–Shell structure in phenyl-grafted carbon nitride/TiO_2 nanohybrids for visible-light-mediated H_2 production with simultaneous rhodamine B degradation. ACS Appl. Nano Mater. 8, 1683–1699.

Hazra, M., Corpino, R., Ricci, P.C., 2026. Windows into planetary science: a review of advances in raman spectroscopy, laser-induced breakdown spectroscopy, and photoluminescence spectroscopy for remote sensing applications. ACS Appl. Opt. Mater. 4, 1560–1592. https://doi.org/10.1021/acsaom.6c00053.

He, F., Jeon, W., Choi, W., 2021. Photocatalytic air purification mimicking the self-cleaning process of the atmosphere. Nat. Commun. 12, 2528.

Hejazi, M.-A., et al., 2024. Novel carbon quantum dots enhanced carbon nanotubes-graphene hybrid nanocomposite for VOCs detection. Diam. Relat. Mater. 148, 111438.

Higazy, S.A., Selim, M.S., El-Segaey, A.A., El-Azabawy, O.E., 2025. Super-protective graphitic carbon nitride nanocomposites as durable surface coatings. Prog. Org. Coat. 205, 109283.

Holmberg, J.P., Ahlberg, E., Bergenholtz, J., Hassellöv, M., Abbas, Z., 2013. Surface charge and interfacial potential of titanium dioxide nanoparticles: experimental and theoretical investigations. J. Colloid Interface Sci. 407, 168–176.

Hu, K., et al., 2011. Adsorptive separation and photocatalytic degradation of methylene blue dye on titanate nanotube powders prepared by hydrothermal process using metal Ti particles as a precursor. J. Hazard. Mater. 192, 514–520.

Ishaq, T., et al., 2024. Recent strategies to improve the photocatalytic efficiency of TiO2 for enhanced water splitting to produce hydrogen. Catalysts 14, 674.

Khan, R., et al., 2025. Phase transition and bandgap modulation in TiO2 nanostructures for enhanced visible-light activity and environmental applications. Sci. Rep. 15, 20309.

Khannyra, S., Luna, M., Gil, M.L.A., Addou, M., Mosquera, M.J., 2022. Self-cleaning durability assessment of TiO2/SiO2 photocatalysts coated concrete: effect of indoor and outdoor conditions on the photocatalytic activity. Build. Environ. 211, 108743.

Kim, D., et al., 2022. Simultaneous assessment of organophosphate flame retardants, plasticizers, trace metals, and house dust mite allergens in settled house dust. Indoor. Air. 32.

Kokkotos, S., Vasilaki, E., Sygellou, L., Vamvakaki, M., Klini, A., 2025. Graphitic carbon nitride (g-C3N4) optical sensors for environmental monitoring. Diam. Relat. Mater. 155, 112301.

Kovalevskiy, N.S., Lyulyukin, M.N., Selishchev, D.S., Kozlov, D.V., 2018. Analysis of air photocatalytic purification using a total hazard index: effect of the composite TiO2/zeolite photocatalyst. J. Hazard. Mater. 358, 302–309.

Krishnan, P., Zhang, M.-H., Yu, L.E., 2018. Removal of black carbon using photocatalytic silicate-based coating: laboratory and field studies. J. Clean. Prod. 183, 436–448.

Lee, M.C., Choi, W., 2002. Solid phase photocatalytic reaction on the soot/TiO_2 interface: the role of migrating OH radicals. J. Phys. Chem. B 106, 11818–11822.

Li, M., et al., 2025. MWCNTs-OH-modified AgInS2 for highly efficient visible-light degradation of gaseous formaldehyde. Diam. Relat. Mater. 157, 112571.

Li, Q., Li, F., 2021. Recent advances in molecular oxygen activation via photocatalysis and its application in oxidation reactions. Chem. Eng. J. 421, 129915.

Li, Z., Meng, X., 2020. New insight into reactive oxidation species (ROS) for bismuth-based photocatalysis in phenol removal. J. Hazard. Mater. 399, 122939.

Liu, S.-H., Lin, W.-X., 2019. A simple method to prepare g-C3N4-TiO2/waste zeolites as visible-light-responsive photocatalytic coatings for degradation of indoor formaldehyde. J. Hazard. Mater. 368, 468–476.

Mai, J.-L., Yang, W.-W., Zeng, Y., Guan, Y.-F., Chen, S.-J., 2024. Volatile organic compounds (VOCs) in residential indoor air during interior finish period: sources, variations, and health risks. Hyg. Environ. Health Adv. 9, 100087.

Mayouf, H.J., Naief, M.F., Mohammed, S.N., Mohammed, A.M., 2025. Synthesize and characterization of Fe2O3 nanoparticles and its potential as a photocatalyst. J. Organomet. Chem 1029, 123543.

Mehta, S.S., et al., 2023. Indoor wood-burning from stoves and fireplaces and incident lung cancer among Sister Study participants. Environ. Int. 178, 108128.

Mills, A., O'Rourke, C., Lawrie, K., Elouali, S., 2014. Assessment of the activity of photocatalytic paint using a simple smart ink designed for high activity surfaces. ACS Appl. Mater. Interfaces 6, 545–552.

Misra, V., Singh, V., Singh, A., Kumar, D., Sharma, S.K., 2023. Photocatalytic degradation of methylene blue dye in aqueous solution under UV irradiation using NdMnO3:rGO hybrid nanocomposites as a photocatalyst. Appl. Surf. Sci. Adv. 18, 100491.

Mo, J., Zhang, Y., Xu, Q., Yang, R., 2009. Effect of TiO2/adsorbent hybrid photocatalysts for toluene decomposition in gas phase. J. Hazard. Mater. 168, 276–281.

Munafò, P., Quagliarini, E., Goffredo, G.B., Bondioli, F., Licciulli, A., 2014. Durability of nano-engineered TiO2 self-cleaning treatments on limestone. Constr. Build. Mater. 65, 218–231.

Myakala, S.N., et al., 2024. Harnessing a Ti-based MOF for selective adsorption and visible-light-driven water remediation. J. Mater. Chem. Mater. 12, 19924–19934.

Nagarajan, V., Chandiramouli, R., 2019. γ-graphyne nanotube as nanofilter for cigarette smoke based on chemisorption properties – A first-principles study. Diam. Relat. Mater. 97, 107436.

Nanni, E.J., Lovette, M.E., Hicks, R.D., Fowler, K.W., Borgerding, M.F., 1990. Separation and quantitation of monovalent anionic and cationic species in mainstream cigarette smoke aerosols by high-performance ion chromatography. J. Chromatogr. Sci. 28, 432–436.

Nimmy, A.V., Anandakumar, V.M., Biju, V., 2025. Enhancing the visible-light sensitive photocatalysis of anatase TiO2 through surface-modification. Discov. Mater. 5, 45.

Ong, G.M.C., Gallegos, A., Wu, J., 2020. Modeling surface charge regulation of colloidal particles in aqueous solutions. Langmuir 36, 11918–11928.

Porcu, S., et al., 2020a. Come to light: detailed analysis of thermally treated phenyl modified Carbon Nitride Polymorphs for bright phosphors in lighting applications. Appl. Surf. Sci. 504, 144330.

Porcu, S., et al., 2020b. Highly efficient visible light phenyl modified carbon nitride/TiO2 photocatalyst for environmental applications. Appl. Surf. Sci. 531, 147394.

Porcu, S., et al., 2023. Visible light-mediated inactivation of H1N1 virus UsingPolymer-based heterojunction photocatalyst. Polym. (Basel) 15, 2536.

Porcu, S., Secci, F., Ricci, P.C., 2022. Advances in hybrid composites for photocatalytic applications: a review. Molecules 27, 6828.
Roongraung, K., Cherevan, A., Eder, D., Chuangchote, S., 2023. Correction: CdS/TiO $_2$ nanostructures synthesized *via* the SILAR method for enhanced photocatalytic glucose conversion and simultaneous hydrogen production under UV and simulated solar irradiation. Catal. Sci. Technol. 13, 5785.
Samuel, O., et al., 2022. WO3–based photocatalysts: a review on synthesis, performance enhancement and photocatalytic memory for environmental applications. Ceram. Int. 48, 5845–5875.
Sangkham, S., et al., 2024. An update on adverse health effects from exposure to PM2.5. Environ. Adv. 18, 100603.
Sheoran, K., et al., 2022. Air pollutants removal using biofiltration technique: a challenge at the frontiers of sustainable environment. ACS Eng. Au 2, 378–396.
Shimazu, H., 2016. Determination of polycyclic aromatic hydrocarbons in cigarettes and cigarette smoke. Environ. Pollut. 5, 15.
Singh, S., Vishwakarma, P., Gupta, T., 2024. Review of current and future indoor air purifying technologies. ACS ES&T Eng. 4, 2607–2630.
Soleimani, F., Dobaradaran, S., De-la-Torre, G.E., Schmidt, T.C., Saeedi, R., 2022. Content of toxic components of cigarette, cigarette smoke vs cigarette butts: a comprehensive systematic review. Sci. Total Environ. 813, 152667.
Stagi, L., Chiriu, D., Carbonaro, C.M., Corpino, R., Ricci, P.C., 2016. Structural and optical properties of carbon nitride polymorphs. Diam. Relat. Mater. 68, 84–92.
Stefanakis, D., Krasoudaki, T., Kaditis, A.-I., Bakolas, A., Maravelaki, P.-N., 2021. Design of novel photocatalytic films for the protection of architectural surfaces via the incorporation of green photocatalysts. Coatings 11, 934.
Talaie, A., Fulazzaky, M.A., Rezania, S., Tamadon, A., 2026. Adsorption, catalytic oxidation, and phytoremediation for air pollution control: a comprehensive review. Environ. Sci.: Atmos. 6, 27–46.
Tang, S., et al., 2024. Advances in TiO2-enhanced photocatalytic building materials: applications in cement and asphalt for environmental purification. Low-carbon Mater. Green Constr. 2, 26.
Vasiljević, B.R., et al., 2025. Designing innovative ZnPc/N-CQDs hybrid material as efficient photocatalyst for environmental remediation. Ceram. Int. 51, 29416–29425.
Vu, A.T., et al., 2015. Polycyclic aromatic hydrocarbons in the mainstream smoke of popular U.S. Cigarettes. Chem. Res. Toxicol. 28, 1616–1626.
Walhout, P.K., He, Z., Dutagaci, B., Nawrocki, G., Feig, M., 2022. Molecular dynamics simulations of rhodamine B zwitterion diffusion in polyelectrolyte solutions. J. Phys. Chem. B 126, 10256–10272.
Wang, C.-Y., et al., 2026. Metal-organic framework-derived carbons coupled CdSe quantum dots for solar H2 production beyond visible region. Appl. Catal. B: Environ. Energy 390, 126552. https://doi.org/10.1016/j.apcatb.2026.126552.
Wang, W., et al., 2021. Insoluble matrix proteins from shell waste for synthesis of visible-light response photocatalyst to mineralize indoor gaseous formaldehyde. J. Hazard. Mater. 415, 125649.
Wang, Y., et al., 2022. A warm-white light-emitting diode based on single-component emitter aromatic carbon nitride. Nat. Commun. 13, 6495.
Weon, S., He, F., Choi, W., 2019. Status and challenges in photocatalytic nanotechnology for cleaning air polluted with volatile organic compounds: visible light utilization and catalyst deactivation. Environ. Sci. Nano 6, 3185–3214.
Wheeler, A.J., et al., 2014. Impacts of air cleaners on indoor air quality in residences impacted by wood smoke. Environ. Sci. Technol. 48, 12157–12163.
Wood Smoke and Your Health, 2025. U. S. Environ. Prot. Agency.
Wu, J., Alipouri, Y., Luo, H., Zhong, L., 2022. Ultraviolet photocatalytic oxidation technology for indoor volatile organic compound removal: a critical review with particular focus on byproduct formation and modeling. J. Hazard. Mater. 421, 126766.
Xiao, Y.-Z., Mohammed, A.A.K., Kuo, S.-W., EL-Mahdy, A.F.M., 2025. Innovative β-ketoenamine-linked covalent organic frameworks: tailored D1-A-D2-A structure for highly efficient photocatalytic degradation of organic pollutants. Sep. Purif. Technol. 356, 129950.
Xin, W., Zhu, D., Liu, G., Hua, Y., Zhou, W., 2012. Synthesis and characterization of Mn–C–Codoped <math id="M1"><mrow><msub><mrow><mtext>TiO</mtext></mrow><mn mathvariant="bold">2</mn></msub></mrow></math>nanoparticles and photocatalytic degradation of methyl Orange dye under sunlight irradiation. Int. J. Photoenergy 2012, 1–7.
Xue, X., et al., 2012. Raman investigation of nanosized TiO $_2$: effect of crystallite size and quantum confinement. J. Phys. Chem. C 116, 8792–8797.
Yaacob, N.A., et al., 2026. Recent advances on photocatalytic geopolymer on the degradation of organic pollutants: a review. J. Hazard. Mater. Adv. 21, 100946.
Yang, J., et al., 2023. Enhancing visible-light photocatalytic performance of Au/TiO $_2$ catalysts through light reflection-promoted optical absorption with oriented anatase mesocrystals. J. Mater. Chem. Mater. 11, 4751–4757.
Yang, J., et al., 2025a. A comprehensive review on indoor air pollutants and their health impacts: priority pollutants and suggested mitigations. Air Qual. Atmos. Health 18, 2151–2184.
Yang, Y., Kuang, J., Cao, W., 2025b. In Situ hydrothermal synthesis of Schottky compound Ti $_2$ CT $_x$ /TiO $_2$ for efficient photocatalytic oxidation NO $_x$ removal. J. Phys. Chem. C 129, 1702–1713.
Yi, G., et al., 2024. Degradation of indoor formaldehyde by the flexible porous material loaded photocatalyst. J. Environ. Chem. Eng. 12, 111823.
Yola, M.L., Eren, T., Atar, N., 2014. A novel efficient photocatalyst based on TiO2 nanoparticles involved boron enrichment waste for photocatalytic degradation of atrazine. Chem. Eng. J. 250, 288–294.
Zhao, J., et al., 2023. A new Cd(II)-based coordination polymer for efficient photocatalytic removal of organic dyes. Molecules 28, 6848.